

## 8. SITE 916<sup>1</sup>

### Shipboard Scientific Party<sup>2</sup>

#### HOLE 916A

**Date occupied:** 7 October 1993  
**Date departed:** 9 October 1993  
**Time on hole:** 2 days, 7 hr, 15 min  
**Position:** 63°29.137'N, 39°48.400'W  
**Bottom felt (drill-pipe measurement from rig floor, m):** 523.2  
**Distance between rig floor and sea level (m):** 10.89  
**Water depth (drill-pipe measurement from sea level, m):** 513.7  
**Total depth (from rig floor, m):** 624.9  
**Penetration (m):** 101.7  
**Number of cores (including cores having no recovery):** 15  
**Total length of cored section (m):** 101.7  
**Total core recovered (m):** 16.86  
**Core recovery (%):** 16.6  
**Oldest sediment cored:**  
Depth (mbsf): 101.7  
Nature: volcanoclastic breccia  
Age: early to middle Eocene (?)  
Measured velocity (km/s): 1.8

**Comments:** Unable to enter hole after bit change.

**Principal results:** Site 916 (proposed Site EG63-1B) is located on the East Greenland Shelf, approximately 50 km from the coast. This site was selected to penetrate a representative sequence of Quaternary and Tertiary sediments, commensurate with deep penetration of the feathered edge of the seaward-dipping reflector sequences (SDRS). The primary scientific objectives of this site are (1) the glacial history of Quaternary and Holocene time; (2) the Paleogene sedimentation and subsidence history, and (3) the composition, age, and eruption environment of the SDRS.

Lithologic Unit I (0–78.6 mbsf, maximum thickness) comprises glaciomarine sediments and diamicton (Fig. 1). Very poor recovery of this unit precluded our obtaining an accurate thickness from the recovered core. Nevertheless, the unit has been subdivided into three subunits. The upper subunit (IA: 0–15 mbsf) consists of gravel-sized fragments of basalt, dolerite, gabbro, and metamorphic rocks. The middle subunit (IB: 15–33 mbsf) is a compact, heterolithic diamicton that has been interpreted as a lodgement till that was deposited by a thick, grounded ice sheet. Clasts include metamorphic and igneous rocks. Only gravel was recovered from Subunit IC (from 33 to as much as 78.6 mbsf). The lower part of the diamicton gives a Quaternary age on the basis of foraminifers.

Lithological Unit II (78.6–97 mbsf) is dominated by volcanoclastic sandy silt with interbeds of silty sand. Siderite-rich layers form distinct light-colored beds 1 to 10 mm thick. Episodic deposition is recorded by small scale fining-upward sequences, cross laminae, convolute laminae, and load casts. Three meso-scale coarsening-upward sequences were

observed. We found well-preserved fragments of wood and rootlets in Section 152-916A-14R-1. The absence of marine microfauna and the abundance of woody fragments indicate that this sediment was deposited in a deltaic setting in a nearshore environment, but we were unable to determine whether it was marine, lagoonal brackish, or lacustrine. Future shore-based studies may resolve this question. We also were unable to date lithologic Unit II; it has been tentatively assigned an early to middle Eocene age on the basis of seismic stratigraphic correlation with Sites 915 and 917.

Lithologic Unit III (97–102 mbsf, total depth) is a volcanic breccia with olivine-rich basalt present as in-situ layers or large clasts of local origin. The breccia may represent a lahar or volcanic mud flow. The olivine in the basalt has been replaced by iddingsite.

Bedding planes dip at 10° to 30° throughout lithologic Unit II, and the core has been faulted normally in several places. This is consistent with observations of the seismic profiles, which indicate a normal fault in the vicinity of Hole 916A. A 20-cm-wide zone of alteration in Unit III (Section 152-916A-15R-2, 97.5 mbsf), tentatively thought to represent hydrothermal activity, also is consistent with faulting.

Sections 152-916A-4R-2, and -5R-1 from lithologic Subunit IB exhibit normal magnetization. No biostratigraphic data are available for these cores; however, Core 152-916A-9R yielded a Pleistocene age. Correlation with the Brunhes Chron is proposed. Sedimentary rocks from lithologic Units II and III also show normal polarity magnetization, but no biostratigraphic data are available for these units; thus, assignment of a magnetochron was not possible for these cores.

No significant amounts of methane (C<sub>1</sub>) or ethane (C<sub>2</sub>) were detected for sediment from Hole 916A. Total organic carbon (TOC) values for the sediment range from 0 to 57 wt%, which reflects variation in the amount of plant debris. Carbon-nitrogen (C/N) ratios are higher than 12 for the siltstone and the brown coal of lithologic Unit II, which is characteristic of terrigenous organic material. In addition, the organic matter contains mainly type III kerogen and has been provisionally interpreted as having a terrigenous provenance, although this interpretation must be treated with caution until the contribution from thermal maturation and aquatic algal material has been assessed completely. Deposition under anaerobic conditions in the aquatic environment prevented the decomposition of the organic material, as indicated by well-preserved plant fossils and authigenic pyrite and siderite found in the sediment.

Principal findings at Site 916 include the following:

1. Basaltic basement occurs just below a depth of 101.7 mbsf, predicted by the sharp reflector observed in seismic profiles.
2. The basalt was emplaced as a lava flow and probably was weathered in a subaerial environment.
3. The basement is overlain by sediment having high volcanoclastic and organic matter components and was deposited in either a marine, a marginal marine, or a lacustrine deltaic environment.
4. Although it was not possible to determine the age of the lower sedimentary units, we anticipate that these will yield diagnostic microfossils (e.g., palynomorphs) during shore-based studies. These studies will be required to determine the minimum age of the last volcanic rocks and the subsequent subsidence history of the margin.
5. As with Sites 914 and 915, the presence of diamicton confirms that wet-based glaciers advanced to at least this point on the shelf, about 53 km east of the present ice sheet.

<sup>1</sup> Larsen, H.C., Saunders, A.D., Clift, P.D., et al., 1994. *Proc. ODP, Init. Repts.*, 152: College Station, TX (Ocean Drilling Program).

<sup>2</sup> Shipboard Scientific Party is as given in list of participants preceding the contents.

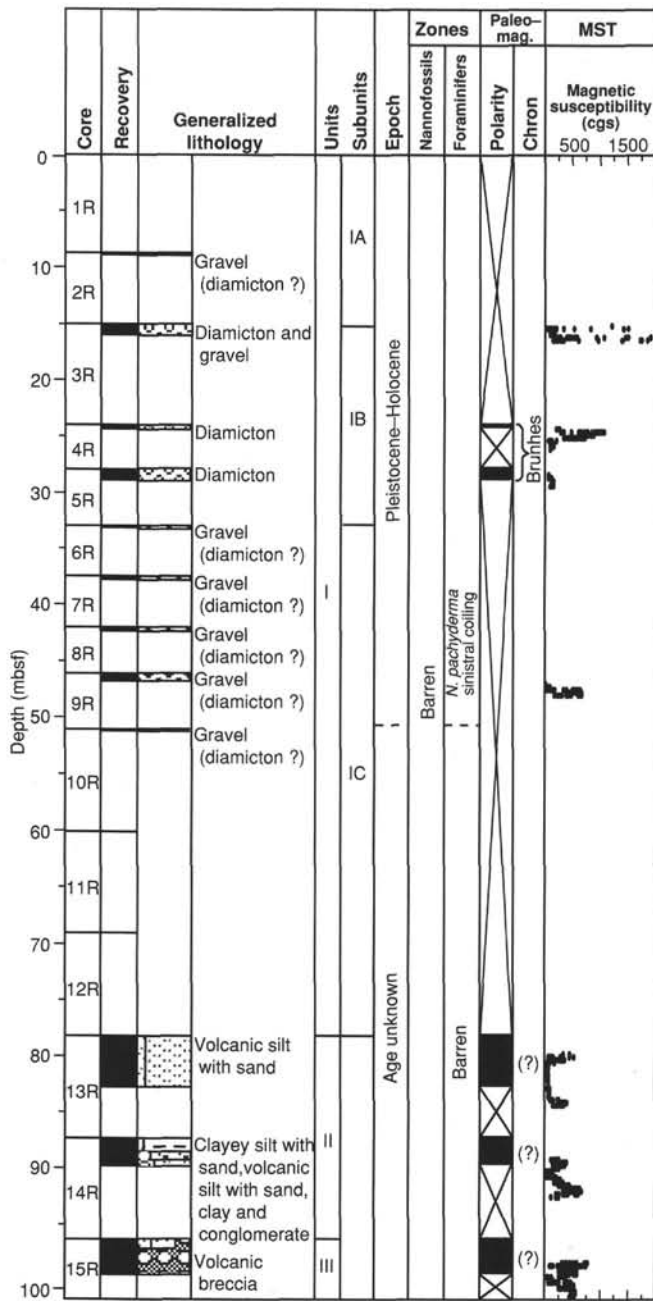


Figure 1. Site summary for Site 916.

**OPERATIONS**  
**Hole 916A**

After the ship was offset to site-survey location EG63-1B, a Ben-thos shallow-water beacon was deployed (Model 210 LP, 14.5 kHz, 190 dB, serial number 44656) at 1615 hr (all times are Universal Time Coordinated [UTC] unless otherwise specified) on 7 October. A back-up beacon (Datasonics, Model 354B, 16.5 kHz, serial number 763) was deployed at 1730 hr. After the ship stabilized over the beacon, a rotary core barrel (RCB) bottom-hole assembly (BHA), having a new C-4 RBI bit and without a mechanical bit release, was run in, and Hole 916A was spudded at 1830 hr on 7 October. The depth of the water was determined as 513.7 m.

RCB-coring advanced to 101.7 mbsf by 0345 hr on 9 October. A record of the coring process at Site 916 is shown in Table 1. Although

Table 1. Coring summary, Site 916.

Core	Date (Oct. 1993)	Time (UTC)	Depth (mbsf)	Length cored (m)	Length recovered (m)	Recovery (%)
				500	1500	
152-916A-						
1R	7	2100	0.0-8.8	8.8	0.11	1.3
2R	8	0050	8.8-15.1	6.3	0.25	4.0
3R	8	0630	15.1-24.1	9.0	1.05	11.6
4R	8	0945	24.1-28.1	4.0	1.40	35.0
5R	8	1200	28.1-33.2	5.1	1.01	19.8
6R	8	1340	33.2-37.7	4.5	0.15	3.3
7R	8	1520	37.7-42.2	4.5	0.28	6.2
8R	8	1640	42.2-46.3	4.1	0.35	8.5
9R	8	1750	46.3-51.3	5.0	0.80	16.0
10R	8	1900	51.3-60.4	9.1	0.15	1.7
11R	8	2000	60.4-69.4	9.0	0.00	0.0
12R	8	2245	69.4-78.6	9.2	0.00	0.0
13R	9	0030	78.6-87.7	9.1	4.53	49.8
14R	9	0215	87.7-96.7	9.0	3.51	39.0
15R	9	0445	96.7-101.7	5.0	3.27	65.4
Coring totals:				101.7	16.86	16.6

the bit had accumulated only 23 hr, the drilling team felt it prudent to pull the bit to investigate its condition after the premature failure of the same type of bit at Hole 915A. A second free-falling funnel (FFF) was prepared and launched at 0530 hr on 9 October. The vibration-isolated television camera was deployed, which verified that the FFF was upright.

**Reentry Number 1**

A new RBI C-7 bit was affixed to the BHA and three extra drill collars were added to improve deep basement coring. At 1330 hr on 9 October, the FFF was entered. The bit encountered a hard bridge at 6.8 mbsf, and for the next 3 hr, the drilling team attempted to wash and ream past this obstruction. Their efforts were hampered by their inability to add more than 5 kips weight on bit, because the BHA was still above the mudline. After advancing to only 13.8 mbsf during this period, the drilling team abandoned their effort to reenter the hole. The BHA then was tripped to the surface and arrived back on deck at 2330 hr on 9 October. It was subjected to a wet particle inspection to ensure that none of its connections were cracked as a result of our unsupported spudding attempt.

**LITHOSTRATIGRAPHY**

**Introduction**

Site 916, situated in 512 m of water, is the third in a series of localities drilled along a short (6 km) east-west transect near the middle to outer part of the East Greenland continental shelf. The section at Site 916 was divided into three lithologic units:

1. Unit I is an upper, glaciogenic unit of Quaternary age.
2. Unit II is a lower Tertiary volcanioclastic sequence, possibly of Oligocene to Eocene age (Table 2; Fig. 2).
3. Unit III is a volcanic breccia. No direct age-control could be obtained from the core, and age estimates depended in part on correlations with other cores along the transect and regional seismic stratigraphy.

Lithologic Unit I comprises three subunits. Subunit IA (0-15.1 mbsf) consists of gravel, and includes igneous, metamorphic, and sedimentary rock fragments. By correlation with lithologic Subunit IA at Sites 914 and 915, Subunit IA was probably deposited as dropstones by ice-rafting during the late Pleistocene and Holocene. Subunit IB (15.1-33.2 mbsf) includes compact, heterolithic diamicton and has been interpreted as lodgement till deposited by grounded ice. Some gravel was also recovered within Subunit IB, and this probably was washed from the diamicton. The lower Subunit IC was recovered between 33.2 and 60.4 mbsf, but only gravel was recovered. These lower gravels are

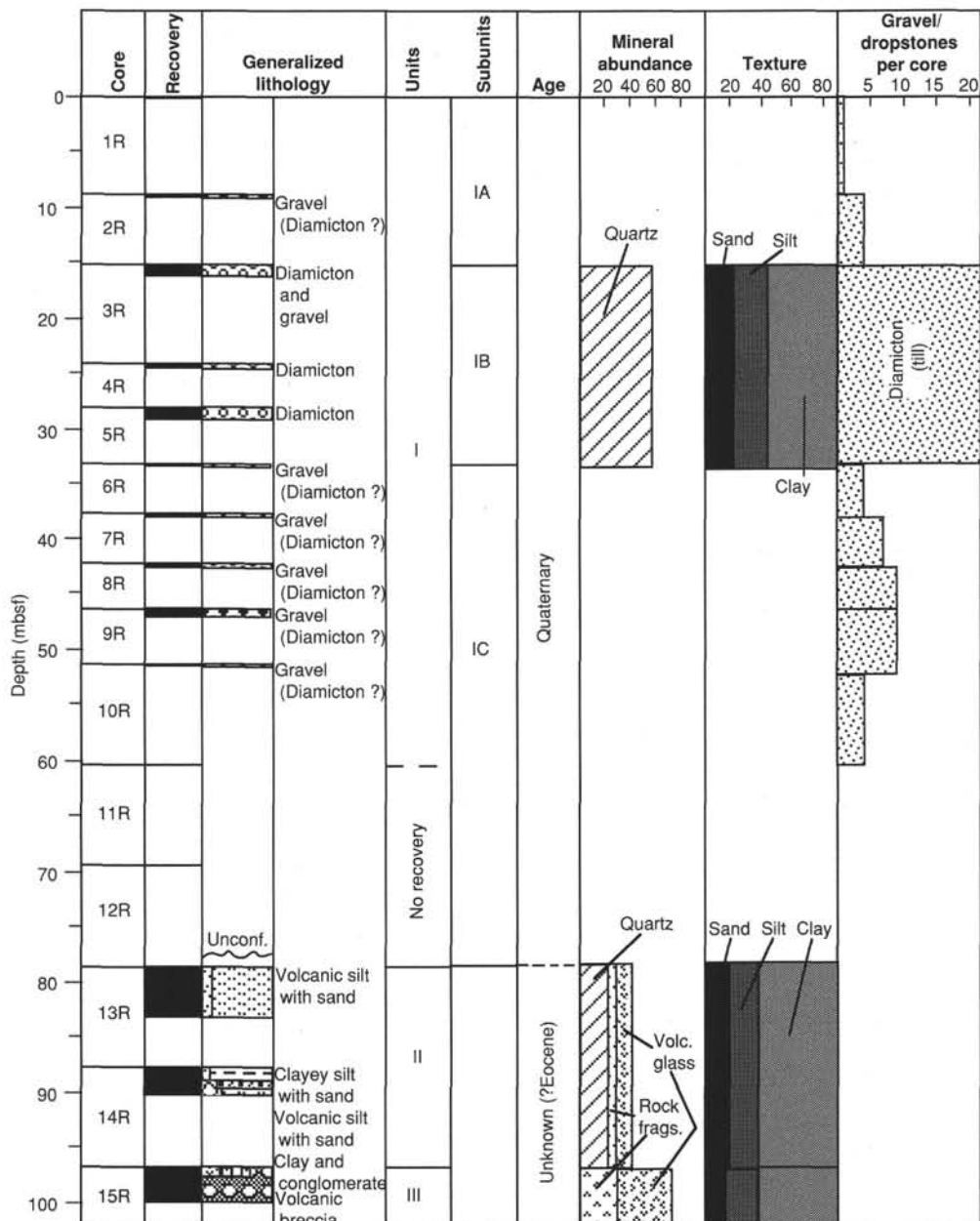


Figure 2. Lithostratigraphic summary of Site 916, East Greenland Margin. Mineral abundance and texture from smear-slide analyses. Average values shown for units. A count of gravel/dropstones was based on all clasts larger than 1 cm. No marine microfossils were found in this part of the core.

Table 2. Summary of lithologic units, Site 916.

Lithologic unit	Lithology	Depth (mbsf)	Core, intervals	Thickness (m)	Age
I	Glaciomarine mud with dropstones and diamicton (till)	0–78.6 (max)	152-916A-1R-1 to -10R	78.6	Quaternary
IA	Gravel	0–15.1	152-916A-1R-1 to -2R	15.1	Quaternary
IB	Compacted diamicton (till)	15.1–33.2	152-916A-3R to -5R	18.1	Quaternary
IC	Gravel	33.2–78.6 (max)	152-916A-6R to -10R	45.4	Quaternary
Gap	No recovery	60.4–78.6	152-916A-11R to -12R	18.2	??
II	Volcanic silt with silty sand interbeds	78.6–96.7	152-916A-13R to -14R	18.1	Unknown; presumed Eocene or Oligocene
III	Volcanic breccia	96.7–101.7	152-916A-15R	5.0	Unknown; presumed middle Eocene

probably reworked from older glaciomarine deposits or, possibly, in part from subglacial, channel deposits associated with the glaciation recorded by Subunit IB. No material was recovered between 60.4 and 78.6 mbsf. Consequently, Unit I may be as much as 78.6 m thick (this is shown in Fig. 2).

Lithologic Unit II is dominated by volcanoclastic sandy silt, with interbeds of silty sand. Sideritic layers form distinct, light-colored beds of 1 to 10 mm thick, and siderite is present as cement throughout the unit. Pyrite is also locally present as small nodules, 2 to 15 mm in diameter. Load clasts, cross-beds, channeling, occasional fining-upward sequences, 3 to 7 cm thick, are present in some parts of the unit, recording episodic deposition. Overall, the unit exhibits three coarsening-upward sequences. Pieces of well-preserved wood, as much as 2 cm long (with some showing preserved annual ring structure), are present in parts of lithologic Unit II. These features suggest deposition of volcanogenic sediments into a deltaic environment.

Lithologic Unit III is a volcanic breccia associated with thin interbedded lava flows. It is composed of altered basalt fragments in a volcanoclastic matrix.

### Lithologic Units

Lithologic Unit I: glaciomarine sediments and diamicton (till)

Interval: Cores 152-916A-1R to -10R

Depth: 0.0–78.6 mbsf

Thickness: 78.6 m

Age: Quaternary

This unit is divided into three subunits: an upper zone, where gravel was recovered, that overlies a thick, compact diamicton, which in turn overlies more gravel.

Lithologic Subunit IA: gravel

Interval: Cores 152-916A-1R to -2R

Depth: 0.0–15.1 mbsf

Thickness: 15.1 m

Age: Quaternary

This subunit comprises washed gravel. Eighteen gravel clasts were recovered that ranged from 4 to 8 cm in diameter, of which nine were basalt. All the remaining rock fragments are igneous and metamorphic and include 28% gneiss and granitic gneiss, 11% diorite, and 6% each of dolerite and quartzite (Fig. 3). This gravel presumably originated as ice-rafted dropstones. This suite of lithologies reflects erosion of Tertiary basalts and Precambrian continental basement by the Greenland Ice Sheet during the late Pleistocene and Holocene. Although small basalt outcrops are thought to occur on the seafloor only a few kilometers west of Site 916, another probable source of this material is the basalt exposure at Kangerdlugssuaq, about 500 km to the north.

Lithologic Subunit IB: compacted diamicton (till)

Interval: Cores 152-916A-3R to -5R

Depth: 15.1–33.2 mbsf

Thickness: 18.1 m

Age: Quaternary

Massive diamicton was recovered from Cores 152-916A-3R, -4R, and -5R. Gravel was recovered with the diamicton and probably represents zones where the diamicton matrix was lost during coring. Where recovered, the diamicton exhibits a preferred fabric both in the core and in thin section (Fig. 4). It is also extremely compact, dewatered, and indurate. Gravel-sized clasts are scattered randomly through the diamicton. Most cobbles are angular, but a few are rounded. The diamicton matrix consists of sandy silt and clay, and numerous grains of quartz, feldspar, and amphibole are present. X-ray diffraction analyses show that the diamicton matrix is composed primarily of quartz and feldspar, with small amounts of amphibole, mica, chlorite, phillipsite, and aragonite.

The lithologies of the clasts in the diamicton strongly suggest a source from East Greenland. Twenty-nine loose rock fragments asso-

ciated with the diamicton were described, together with an additional 17 large clasts incorporated within the diamicton. The clasts indicate that the diamicton was derived primarily from terranes dominated by igneous and metamorphic rocks in eastern Greenland. The sources must include regions composed primarily of Precambrian(?) gneiss, amphibolite, and metasedimentary rocks. In contrast to the overlying glaciomarine sediments of lithologic Subunit IA, basalt constitutes only 10% of the coarse material found within the diamicton (Fig. 5).

The contrasting lithologies of the rock fragments found in lithologic Subunits IA and IB are consistent with the interpretation that Subunit IB is a basal till, as Precambrian crystalline rocks occur widely along the coastline of East Greenland just west of the drill site, while the nearest extensive outcrops of Tertiary volcanic rocks are in the Kangerdlugssuaq region (68°N), more than 500 km away. A basal till might be expected to incorporate mostly local lithologies, while dropstones in Subunit IA may be largely derived from icebergs transported south by the East Greenland Current (Thiede et al., 1990). Eastward flow of the Greenland Ice Sheet to Site 916, therefore, would transport primarily crystalline erratics, although some basalt may have been derived from erosion of nearby submarine basaltic outcrops. However, these are thought to be of limited areal extent, based on seismic profiling.

The XRD data also are consistent with this interpretation, as the presence of phillipsite, a zeolite that generally forms in marine environments, indicates that the diamicton includes a component of material reworked and eroded from older marine sediment. Aragonite is also likely to be of marine origin. Their presence in the diamicton is best explained by subglacial erosion of shelf sediment beneath a grounded ice sheet, and incorporation of the older marine sediment into a basal till.

Lithologic Subunit IC: gravel

Interval: Cores 152-916A-6R to -10R

Depth: 33.2–78.6 mbsf

Thickness: 45.4 m

Age: Quaternary

This interval is characterized by large drilling fragments of igneous and metamorphic rocks that range from 4 to 8 cm in diameter. All associated matrix was presumably washed out during the drilling process. This gravel is thought to have originated as ice-rafted dropstones, although some of it may have originally been associated with the overlying diamicton or with older glacial deposits. Altogether, 34 gravel clasts were recovered, of which 13 (26%) are basalt. The remaining rock fragments are igneous and metamorphic and include gneiss, granitic gneiss, diorite, and dolerite. This suite of lithologies reflects erosion of the Precambrian continental basement by the Greenland Ice Sheet during the late Pleistocene, together with a significant component of Tertiary basalts, which were probably eroded either in the north and transported to the drill site by ice-rafting or are locally derived from submarine outcrops.

Nothing was recovered from Cores 152-916A-11R and -12R, which were drilled to a depth of 78.6 mbsf. Marine and glaciomarine sediment of overlying subunits may continue to this depth.

Lithologic Unit II: volcanic silt with silty sand and sandstone interbeds

Interval: Cores 152-916A-13R to -14R

Depth: 78.6–96.7 mbsf

Thickness: 18.1 m

Age: unknown; presumed early to middle Eocene

The dominant lithology in this unit is a greenish-black, massive, homogeneous volcanoclastic silt. Sand-filled burrows occur intermittently and are locally cemented with pyrite. Some areas are slightly bioturbated. This sediment evidently derived from both volcanic and crystalline continental terranes in East Greenland, because quartz, plagioclase feldspar, amphiboles, and lithic fragments of basalt all were identified in the sediment. Pyrite, basalt fragments, amphibole, pyroxene, wood fragments, and minor amounts of glauconite all contribute to the dark green color of the sediment.

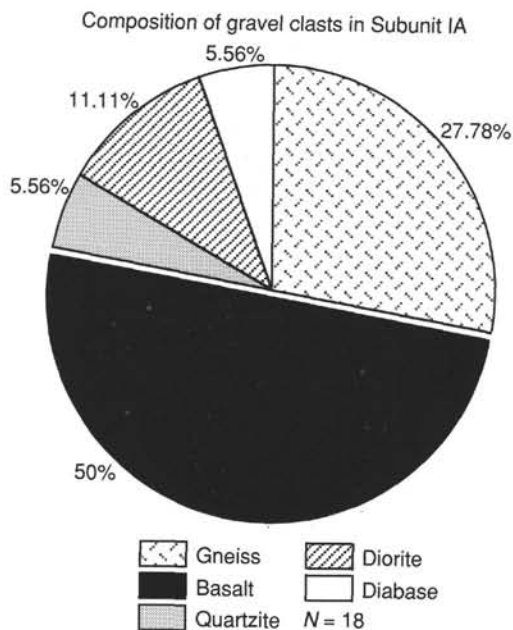


Figure 3. Percentages of basalt and other lithologies found in late Pleistocene and Holocene glaciomarine and ice-rafted debris.

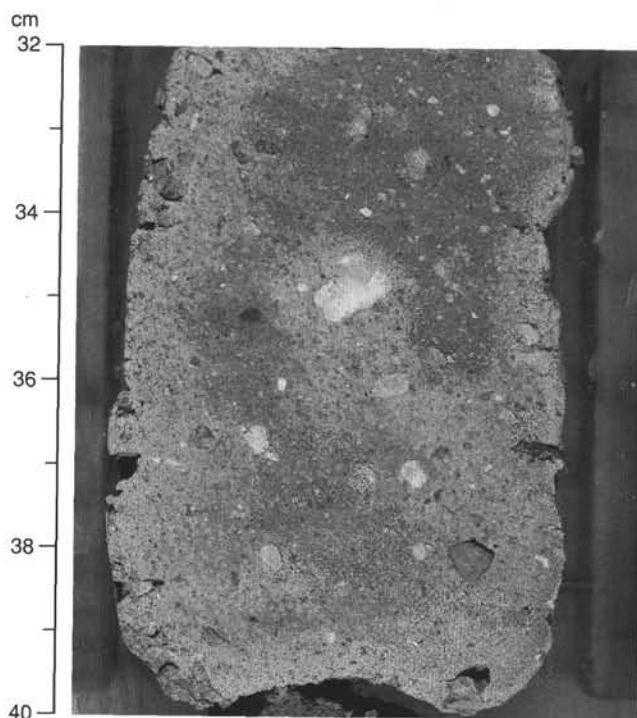


Figure 4. Photograph of diamicton in lithologic Subunit IB, showing the well-developed clast orientation characteristic of basal till (interval 152-916A-3R-1, 32–40 cm).

Prominent, thin, white beds occur in several places within the dark volcanoclastic sediment. The dominant mineral component in the white beds was identified as siderite in smear slides and by XRD. The siderite beds have been somewhat disturbed by burrowing and, locally, were highly disturbed by loading (Fig. 6).

Sandy interbeds occur from approximately 85 to 89 mbsf, generally as alternations with fine sediment, but also as small-scale fining-upward sequences, 3 to 7 cm thick (Fig. 7). Small-scale coarsening-upward beds are also present (Fig. 7), and overall, this unit has three larger-scale coarsening-upward intervals from Cores 152-916A-14R to -13R (see core photos, "Cores" Section, this volume). The bases of the sandy interbeds sometimes exhibit flame structures and ripples 1 to 2 mm high, suggesting that they were deposited rapidly. While fossil wood is common, marine microfossils are conspicuously absent from these beds.

Bedding planes dip at 10° to 30° through lithologic Unit II (Fig. 7). A (normal?) fault having a dip of about 60° and slickensides cuts across Section 152-916A-13R-3, 97–102 cm (82.6 mbsf). This fault offsets an organic-rich horizon against volcanoclastic siltstone. A second set of faults was identified at Section 152-916A-13R-CC, 10 cm, where thinly laminated, siderite-rich beds show several small step faults, each of which has been offset from 2 to 3 mm. The observation of faulting within the core suggests that caution will be needed when interpreting the origin and significance of the prominently dipping bedding planes in Subunit IIA, although the minor extent of deformation and brecciation does not suggest major offset.

The absence of marine microfauna and the abundance of terrigenous woody debris and leaf litter in Subunit IIA suggest that it was deposited in nearshore water, possibly in a delta. In the absence of diagnostic fossils, we cannot ascertain for certain if the environment was marine, lacustrine, or lagoonal and brackish. Future shore-based investigations, perhaps involving palynomorphs, ostracodes, or carbon isotopes of organic residue, may resolve this question. The character of the sediment suggests that it was derived from erosion of a largely volcanic region. The thin sand beds probably reflect episodic, rapid influxes of iron oxide-rich sand into the basin, which was subsequently altered to siderite in a reducing environment.

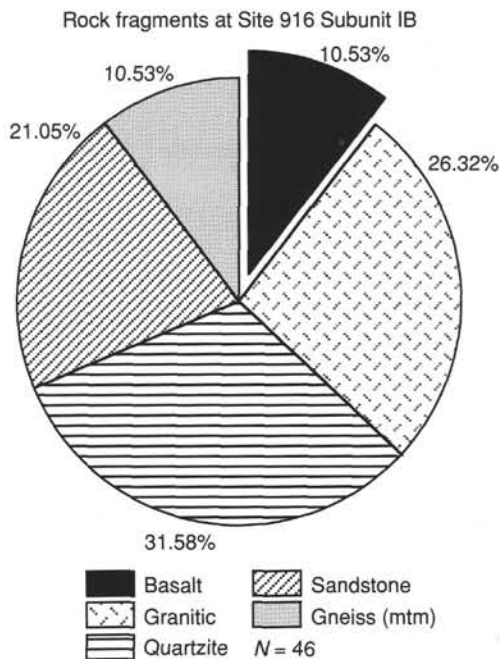


Figure 5. Percentages of basalt and other lithologies found associated with diamicton (basal till).

Lithologic Unit III: volcanic breccia  
 Interval: Core 152-916-15R  
 Depth: 96.7–101.7 mbsf (total depth)  
 Thickness: 5.0 m  
 Age: unknown; presumed early to middle Eocene

Lithologic Unit III consists of a coarse-grained volcanic breccia that was recovered in Core 152-916A-15R. The basalt fragments in the breccia have been altered to various degrees and generally are matrix-supported. Large basalt clasts as much as 30 cm in diameter occur at the base of the core. Several individual basaltic clasts appear to have thin alteration zones or, possibly, cooling rims on their margins. No contact alteration was visible in the matrix at the margins of the clasts in the breccia (Fig. 8), and the matrix has not been sintered or welded, which suggests that the breccia was cool when emplaced. Small faults and slickensides are visible within the breccia matrix. A dendritic calcite-cemented vein extends for 31 cm through the matrix (Fig. 9). This may represent a hydrothermal vein or a highly altered dolerite dikelet. The breccia appears to be a lahar or other type of mass flow deposit. The absence of any quartz in smear slides as well as the absence of nonvolcanic clasts suggest that this breccia deposit was proximal to, and possibly coeval with, lava flows.

### Summary and Conclusions

Lithologic Unit I is a thick, Quaternary age, glaciogenic deposit comprising an upper 15 m of glaciomarine sandy silt with dropstones, a lower 35 m of subglacially derived till, and still lower, 28 m or more of gravel of probable glaciomarine origin. The unit overlies an Eocene(?) volcanoclastic deposit at Site 916. The recovery and recognition of basal till in lithologic Unit I at Site 916 provides further evidence that Pleistocene glaciers advanced through deep water on the continental shelf to this point, about 50 km from the modern coastline. This glaciation may be correlative with the Scoresby Sund glaciation of East Greenland, during which the Greenland Ice Sheet is thought to have extended beyond the modern coastline. The Scoresby Sund glaciation is thought to have occurred during marine isotope stage 6 (Riss/Illinoian), from about 175 to 150 k.y. years ago (Funder, 1989b).

A major unconformity separates the Quaternary sediment from Paleogene volcanoclastic sediment found deeper in Hole 916A. The Tertiary volcanic siltstone is unusually rich in fossil wood, but lacks marine microfossils, so the age of lithologic Unit II is unknown. The sediment was derived from a largely volcanic terrane and deposited in a nearshore, shallow-water environment. Coarsening-upward intervals, abundant woody organic debris, convolute laminae, and fine ripples all suggest that this deposit is deltaic, although it is not known if the setting was marine, lagoonal, or lacustrine. Drilling at Site 916 terminated in a volcanic breccia at 96.7 mbsf, but the structural disruption at the base of the core makes interpretations of the relationship of the Tertiary volcanoclastic sediments and underlying volcanic breccia problematical. Several small (normal?) faults were identified in both lithologic Units II and III, along with a hydrothermal vein in lithologic Unit III.

### BIOSTRATIGRAPHY

#### Calcareous Nannofossils

Only three samples from Hole 916A were available for nannofossil analysis. Sample 152-916A-9R-CC yielded rare specimens of nannofossils. They include *Reticulofenestra bisecta*, *R. daviesii*, *R. umbilicus*, and *R. reticulofenestra reticulata*, an assemblage that suggests a middle Eocene age. These rare specimens probably have been reworked because planktonic foraminiferal data indicate a Quaternary age for this sample. Samples 152-916A-13R-CC and -14R-CC are barren of nannofossils.

#### Planktonic Foraminifers

Only one sample from this site was available for analyzing planktonic foraminifers. Sample 152-916A-9R-CC contains few and moderately preserved specimens of sinistrally coiled *N. pachyderma* and

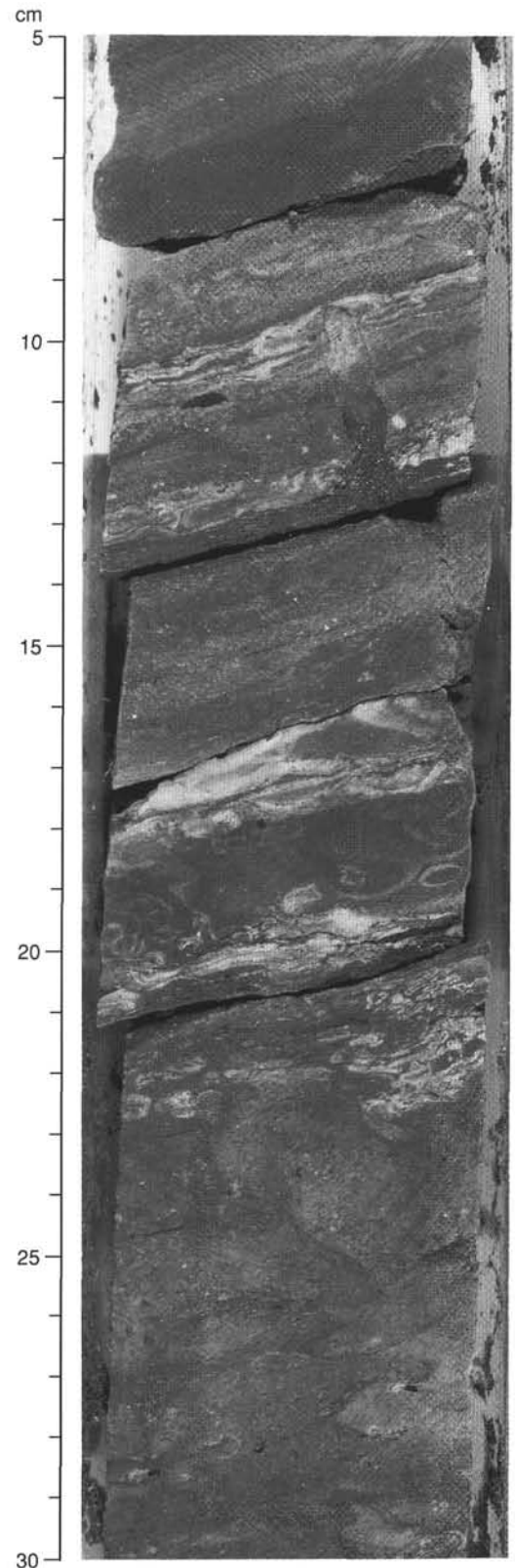


Figure 6. Siderite bands in volcanic silts of lithologic Unit II, Section 152-916A-13R-2. Note the pyrite-filled burrow crossing several siderite bands at 10 cm and convolute siderite bands between 15 and 20 cm. Fine ripples, now convolute, are visible between 8 and 9 cm. Bioturbation is extensive from 22 to 30 cm.

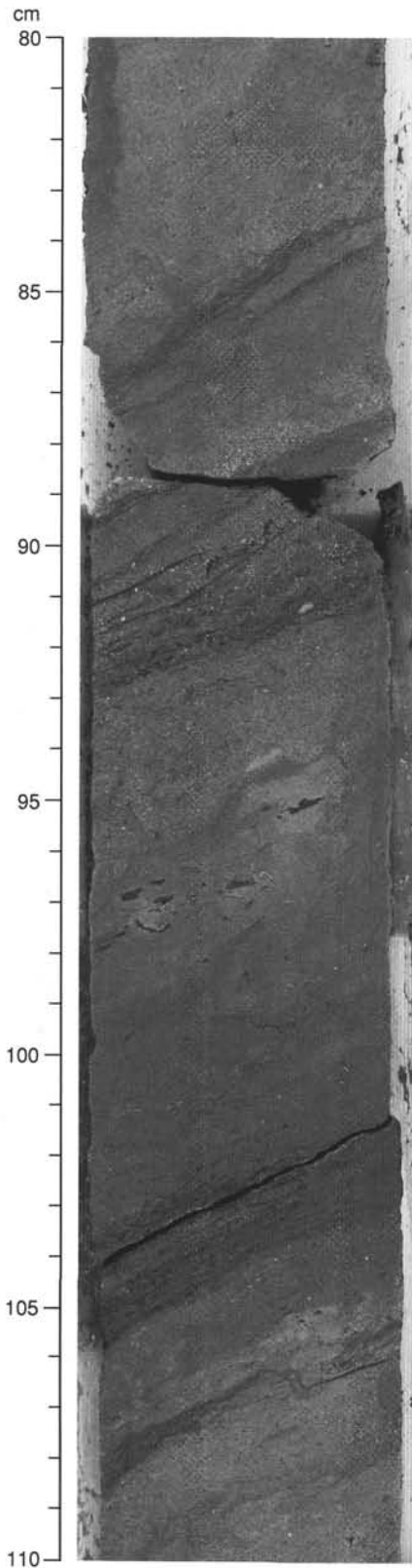


Figure 7. Volcanic silty sandstone and silt of lithologic Unit II, interval 152-916A-13R-2, 80–110 cm. Here, the beds are dipping and a normal fault occurs at 88 to 90 cm. The sediment fines upward from 87 to 83 cm, and coarsens upward from 100 to 91 cm. Dark beds are woody, organic-rich horizons.

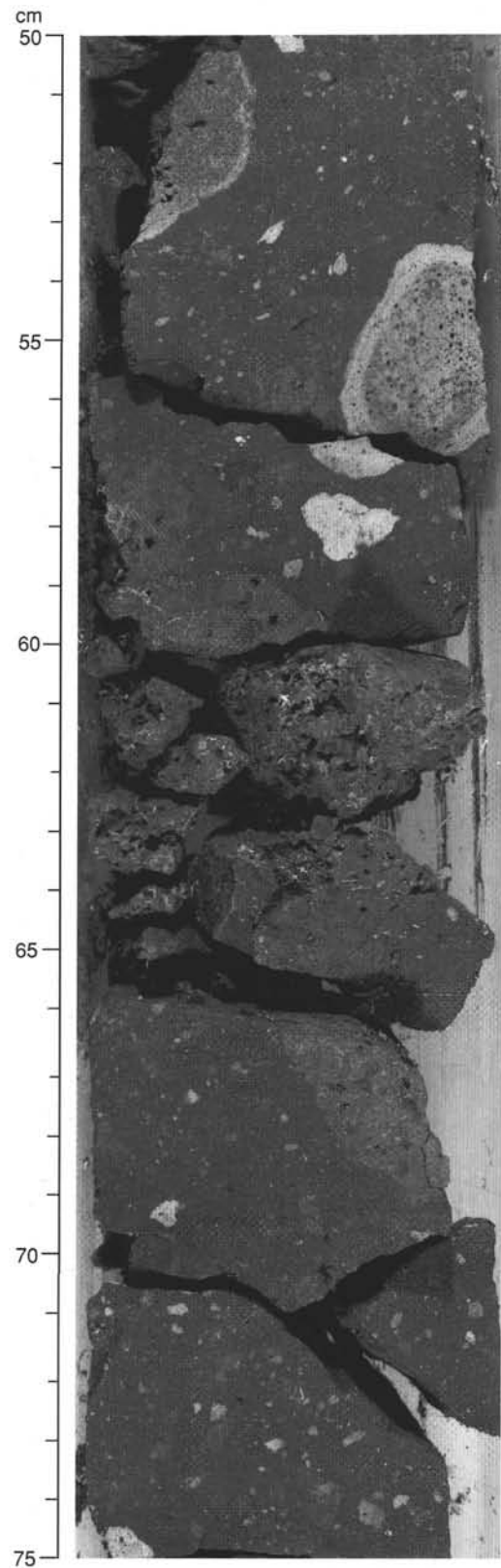


Figure 8. Lithologic Unit III, volcaniclastic breccia, interval 152-916A-14R-2, 50–75 cm. The matrix color is a dusky red, and clasts are various colors, but all derive from a volcanic source area. Note the alteration rims around the clast at 54 to 57 cm. No contact alteration of the matrix was observed, suggesting that this deposit was not sintered or welded, but was emplaced under cool conditions.

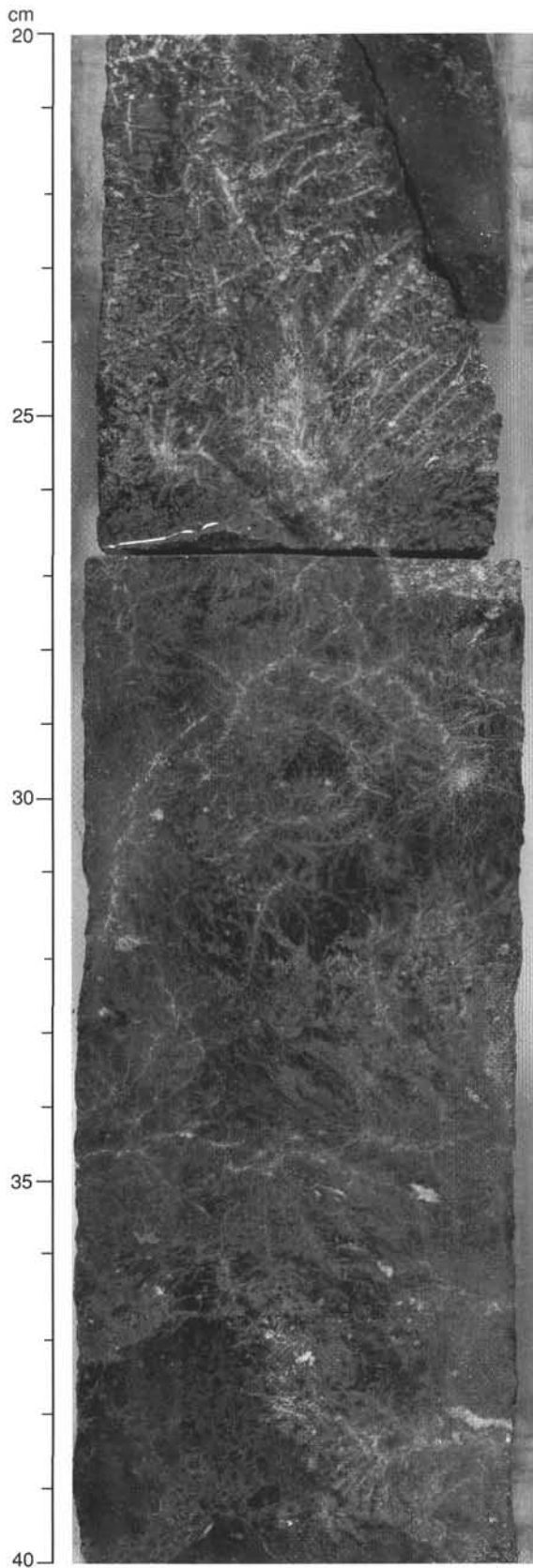


Figure 9. Dendritic calcite emanating from a veinlike structure, cutting across lithologic Unit III (volcaniclastic breccia; interval 152-916A-15R-2, 20–40 cm).

thus can be attributed to the *N. pachyderma* sinistral-coiling Zone, which ranges in age from Pleistocene to Holocene (Fig. 10).

### Benthic Foraminifers

Benthic foraminifers were analyzed from the following intervals and sections: 152-916A-4R-2, 70–72 cm; 152-916A-5R-1, 90–92 cm; 152-916A-9R-CC, and 152-916A-13R-CC to -15R-CC.

Within the recovered Quaternary intervals, Cores 152-916A-1R to -10R; Samples 152-916A-4R-2, 70–72 cm, and -5R-1, 90–92 cm; and Section 152-916A-9R-CC, benthic forms constitute about 40%, 40%, and 70%, respectively, of the total foraminiferal assemblage. Their preservation is moderate. *Cassidulina norvangi*, *Cassidulina teretis*, and *Elphidium excavatum* are common in Samples 152-916A-4R-2, 70–72 cm, and -9R-CC. *Cassidulina teretis* is a dominant species during Pliocene to Pleistocene glacial intervals of the North Atlantic region (Murray, 1984). The assemblage identified in Sample 152-916A-5R-1, 90–92 cm, is dominated by *Cibicides lobatulus*, *Cibicides refulgens* and *Cibicides* spp. and resembles that in Sample 152-915A-1R, 0–2 cm. The latter assemblage has been interpreted to be a post-glacial fauna, because the sample was taken just below the seafloor. However, lower in the succession, in Sample 152-916A-5R-1, 90–92 cm, this same fauna was found intercalated between a characteristic glacial fauna. The assemblage thus has been interpreted to be representative of interglacial periods. Samples 152-916A-13R-CC, 152-916A-14R-CC, and 152-916A-15R-CC are barren of benthic foraminifers (Fig. 10).

### PALEOMAGNETISM

In Hole 916A, paleomagnetic data were obtained from Cores 152-916A-4R, -5R, -13R, and -14R. Diamicton was recovered in Cores 152-916A-4R and -5R. From Cores 152-916A-13R and -14R were recovered shallow marine/lagoonal sands, silts, and mudstones, of probable Eocene age, together with large clasts of basalt. Seismic data (see “Shelf Stratigraphic Summary” chapter, this volume) suggest that Cores -13R and -14R immediately overlie basement. The sediments within Cores 152-916A-13R and -14R have typical dips of 18° to 25°. Paleomagnetic observations are based on WCC analysis of the archive-half sections. The magnetostratigraphy of Hole 916A is summarized in Figure 11.

Sections 152-916A-4R-2 and -5R-1 have initial natural remanent magnetization (NRM) intensities that range between 70 and 240 mA/m. AF demagnetization to 30 mT reduced these intensities to between 10% and 30% of the initial values. Both sections exhibit steep positive inclinations, indicating that they are normally magnetized. No biostratigraphic data are available for these cores; Core 152-916A-9R, however, yielded a Pleistocene age (see “Biostratigraphy” section, this chapter). Correlation with the Brunhes Chron is proposed.

Sedimentary rocks in Sections 152-916A-13R-1 to -13R-3 and 152-916A-14R-1 have initial NRM intensities typically 10 to 100 mA/m. Material from Core 152-916A-15R has NRM intensities that range between 100 and 800 mA/m. AF demagnetization to 30 mT reduced these intensities to between 20% and 30% of the initial values. All sediments in Cores 152-916D-13R to -15R exhibit steep positive inclinations (because of this, we did not apply a tilt correction to the remanence data from each of the core pieces), indicating a normal polarity magnetization. Unfortunately, no biostratigraphic data are available for this sedimentary sequence, and thus, assignment of a magnetochron is not possible for these cores.

### Summary of Paleomagnetic Data from Sites 914, 915, and 916

The sedimentary rocks recovered from Sites 914, 915, and 916 by themselves reveal only a fragmentary geological history for this part of the Southeast Greenland Margin. In all three sites, glacial tills were

recovered that we confidently have assigned to the Brunhes Chron (i.e., are younger than 0.78 Ma). No Neogene rocks were recovered during drilling of these sites. Oligocene and Eocene rocks were recovered in Holes 914B, 915A, and 916A. A number of cores from this interval yielded reliable magnetostratigraphic records. Unfortunately, the paucity of biostratigraphic data from these cores does not permit unambiguous magnetostratigraphic assignments. However, the paleomagnetic studies reveal that the sediments that immediately overlie a carapace of altered volcanic debris, resting on basement in Holes 915A and 916A, are reversed and normally magnetized, respectively, indicating a difference in their ages. Basement rocks recovered from Hole 915A are reversely magnetized. Correlation of these rocks with Chron C24r (which straddles the Paleocene/Eocene boundary) is the best magnetochron estimate (see discussion in "Paleomagnetism" section, "Site 915" chapter, this volume).

### SEDIMENTATION RATES

Mostly pieces of gravel were recovered above the nonmarine sediments and the basement in Hole 916A. No meaningful age-vs.-depth diagram can be constructed for this site because of the lack of useful age information. Some sediments recovered from Core 152-916A-9R (about 47 mbsf), however, yielded a few sinistrally coiled specimens of a planktonic foraminiferal species, *N. pachyderma*, which suggests an age younger than 1.8 Ma. Thus, the sedimentation rate for the interval from seafloor to 47 mbsf is at least 2.6 cm/k.y.

### ORGANIC GEOCHEMISTRY

#### Volatile Hydrocarbons

As required by the shipboard safety and pollution prevention program, concentrations of methane ( $C_1$ ) and ethane ( $C_2$ ) were monitored every core, where sediment was recovered, using standard ODP headspace-sampling techniques. No significant amounts of gases were detected in the sediment column of Site 916.

#### Elemental Analyses

Shipboard sampling at Site 916 was restricted to Cores 152-916A-13R and -14R because of limited core recovery. Fourteen samples were collected from these cores. According to the "Lithostratigraphy" section (this chapter), the sampled sediment sequence consists of grayish-brown sandy siltstone having minor amounts of clay and intercalated coaly peat-type plant fragments. Some samples for shipboard analyses were separated according to lithology into the coaly parts and the surrounding sediments, and these were measured as different samples (Table 3). Three main preliminary lithology types were distinguished: (1) black sandy siltstone with leaves and coaly particles, (2) coaly plant fragments and brown coal bands, (3) volcanoclastic debris flow sediments.

TOC values for the sediments range from 0 to 57 wt% (Table 3). The brown coals and peaty plant fragments show the highest TOC contents (up to 57%), whereas the leaf-bearing siltstones display somewhat lower values of between 1 and 6 wt%. Clearly depleted in organic carbon are the volcanoclastic debris flow sediments, with TOC contents below 0.5 wt%. Significant amounts of carbonate (up to 20 wt%  $CaCO_3$ ) are common in the siltstones and the debris flow sediments (Table 3, Fig. 12). Some of the carbonate may occur as siderite, as indicated by the slow reaction with hydrochloric acid. Siderite was also identified by shipboard XRD analyses (see "Lithostratigraphy" section, this chapter).

In general, sulfur contents are low for the sediments analyzed. Some coaly sediments (extremely enriched in authigenic pyrite, yield sulfur contents of up to 20 wt% (Sample 152-916A-13R-2, 12 cm; Table 3).

### Composition of Organic Matter

Organic matter in the sediments of Hole 916A was characterized using organic carbon/total nitrogen TOC-TN ratios and Rock-Eval pyrolysis data (Table 3). TOC-TN ratios are higher than 12 in the siltstones and the brown coals, which is characteristic of terrigenous organic material (Fig. 12; Bordovskiy, 1965; Emerson and Hedges, 1988). Given the very low organic carbon and nitrogen values, TOC-TN ratios of the debris sediments are not reliable. The pyrolysis data are plotted in a "van Krevelen"-type diagram (Fig. 13). This provides important information about the composition and maturity of the organic matter (e.g., Espitalié et al., 1977; Peters, 1986). The organic matter contains mainly type III kerogen, indicating a terrigenous provenance. Most of the brown coals and peats of Hole 916A are characterized by low hydrogen indexes (HI) and oxygen indexes (OI), which may reflect either a higher thermal maturity for the organic matter or a significant amount of aquatic algal material (kerogen types I or II; Espitalié et al., 1977) in the samples. Thus, these data have to be interpreted with caution, and further analyses, such as kerogen microscopy, will be necessary for a reliable characterization of the organic matter in these brown coals (e.g., Stein, 1991).

### Depositional Environment

The sedimentary sequence of Cores 152-916A-13R and -14R was probably deposited in a lagoonlike shallow-marine or freshwater environment, surrounded by a dense vegetation cover (see "Lithostratigraphy" section, this chapter). Sedimentation of the organic matter-bearing siltstones frequently was interrupted by lava and volcanoclastic debris flows. Seasonal change in vegetation may have led to an intense influx of leaf material and wood fragments. Deposition under anaerobic aquatic conditions prevented the decomposition of the organic material, as indicated by the presence of well-preserved plant fossils and authigenic pyrite crystals. To confirm this preliminary interpretation and to estimate the maturity of the organic matter, shore-based microscopic analyses of the maceral composition will have to be performed.

### INORGANIC GEOCHEMISTRY

At Site 916, only one interstitial-water sample was obtained in the Tertiary section below the diamicton. Methods are described in the "Inorganic Geochemistry" section of the "Explanatory Notes" chapter (this volume). The results obtained are presented in Table 4.

### Synthesis of Data of Sites 914, 915, and 916

In this section, the data obtained from the interstitial-water program at Sites 914, 915, and 916 are discussed in terms of potential processes that have affected the various constituents of the dissolved salts. None of the sites obtained the complete coverage required to describe concentration-depth gradients. This is because of the poor recovery in the glaciogenic sections (see "Lithostratigraphy" sections, "Site 914," "Site 915," and "Site 916" chapters, this volume). However, a composite of the information can be compiled to estimate the potential concentration changes and the processes causing these changes.

Interstitial waters were extracted from samples in the upper few meters of glaciomarine sediments with intermixed dropstones and sparse tephra. The remainder of the fluids come from deeper, sandy and volcanogenic shelf sediments of early Tertiary age. The glaciogenic deposits on top of the older Tertiary sediments were deposited at high rates, probably within a period of considerably less than 2 m.y. (possibly since 0.5 Ma). For example, sedimentation rates in the upper 160 m of Site 914 have been estimated to be more than 9.2 cm/k.y. (see "Biostratigraphy" section, "Site 914" chapter, this volume). Although estimates of the sedimentation rates in the upper sections of Sites 915 and 916 are less certain, it is likely that similar

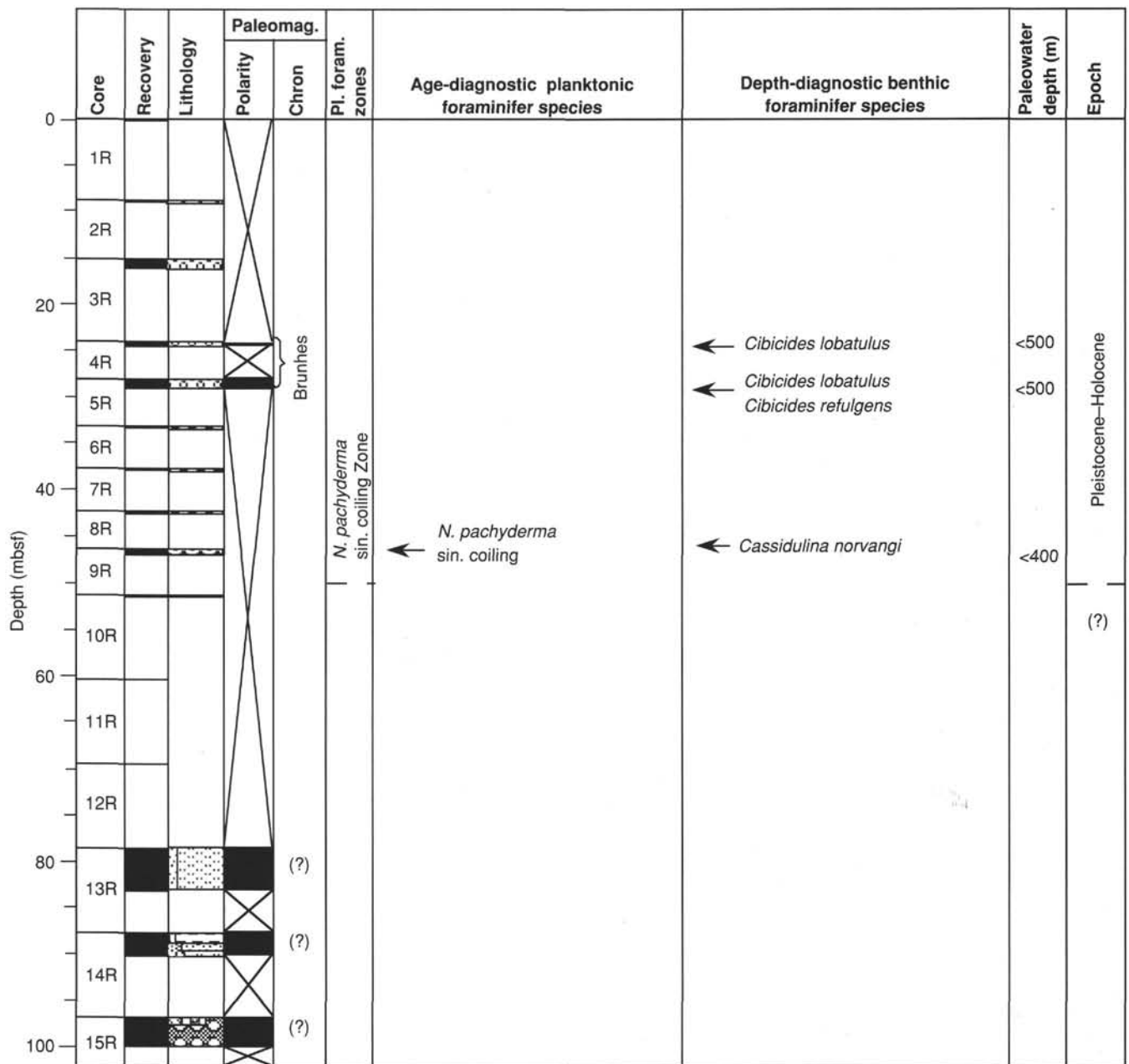


Figure 10. Biostratigraphic summary of Hole 916A. Paleowater depths inferred by benthic foraminiferal species also are shown.

sedimentation rates in the glaciogenic section have prevailed. As a result of these high rates of deposition, communication between the upper and lower deposits may have been hampered. Below, we calculate the approximate diffusive communication lengths, defined by the ratio of two times the diffusion constant (about  $5 \times 10^{-6} \text{ cm}^2/\text{s}$ ) to that of the sedimentation rates (e.g., 5, 10, 50, 100 cm/k.y.):

Sedimentation rate (cm/k.y.)	Communication length (m)
5	600
10	300
30	100
50	60
100	12

Thus, if sedimentation rates are higher than 30 cm/k.y., diffusive communication across the glaciogenic section may have been ham-

pered. However, in the absence of tighter control on sedimentation rate, the data in the above table suggest that a diffusive connection between the upper glaciomarine sediments and the lower Tertiary sediments may have been possible. The absence of interstitial water data in the rapidly deposited glaciogenic sections, however, makes an evaluation of the potential concentration gradients impossible.

In the following passages, we first present the concentration changes with depth after a minimum of interpretation, followed by a short general discussion, and then a summary. The discussion focuses mainly on observations from Sites 914 and 915.

### Observations

Data for alkalinity, sulfate, and ammonium concentrations are presented in Figure 14. Only in the upper part of both sites (i.e., in the glaciomarine sediments) do small increases in alkalinity ( $\text{HCO}_3$ )

Table 3. Summary of organic chemistry analyses at Site 916.

Core, section, interval (cm)	Depth (mbsf)	TC (wt%)	IC (wt%)	TOC (wt%)	CaCO <sub>3</sub> (wt%)	TN (wt%)	TS (wt%)	TOC/N ratio	HI (mgHC/gC)	OI (mgCO <sub>2</sub> /gC)	Lithology
152-916A-											
13R-1, 74-76	79.34	1.98	1.1	0.88	9.16	0.06	0.12	15.63	64	626	Silt, grayish
13R-1, 74-76	79.34	50.10	0.4	49.74	3.00	0.12	2.12	404.39	35	38	Brown coal piece
13R-1, 114-116	79.74	3.14	1.3	1.83	10.91	0.08	0.08	22.86	49	507	Silt, sand, coaly spots
13R-2, 12-14	80.22	3.38	2.0	1.39	16.58	0.03	0.09	46.45	62	725	Silt, leaf coal laminae
13R-2, 12-14	80.22	6.25	0.1	6.16	0.75	0.12	19.56	50.05	70	26	Root piece, massive pyrite
13R-2, 73-75	80.83	2.92	2.0	0.94	16.49	0.05	0.48	20.05	87	696	Silt, coaly spots
13R-3, 48-50	82.08	4.64	1.5	3.12	12.66	0.06	0.00	50.34	53	127	Silt, leaf coal laminae
13R-3, 96-98	82.56	3.97	1.2	2.77	10.00	0.07	0.09	38.36	60	186	Silt, coaly spots
13R-3, 96-98	82.56	57.04	0.0	57.04	0.00	0.13	0.71	452.68	28	11	Coal, pyritized
14R-1, 57-59	88.27	1.39	1.3	0.08	10.91	0.07	0.00	1.15			Volc. sand, altered basalt
14R-1, 137-140	89.70	34.31	0.0	34.31	0.00	0.09	6.79	381.17	111	34	Coaly, dark brown
14R-1, 143-146	89.13	1.16	0.0	1.16	0.00	0.05	0.00	21.43	112	54	Silt, grayish
14R-2, 22-24	89.42	0.70	0.3	0.39	2.58	0.07	0.06	5.94	104	331	Debris flow, red brown
14R-2, 82-84	90.02	2.71	2.3	0.41	19.16	0.07	0.04	5.96			Debris flow, dark brown
14R-2, 150-152	90.70	47.66	0.0	47.66	0.00	0.13	0.55	366.64	52	56	Black coal
14R-3, 25-27	90.95	0.00	0.0	0.00	0.00	0.05	0.00	0.00			Volc. conglomerate

Note: TC = total carbon; IC = inorganic carbon; TOC = total organic carbon; CaCO<sub>3</sub> = calcium carbonate; TN = total nitrogen; TS = total sulfur; TOC/TN = total organic carbon/total nitrogen; HI = hydrogen index; OI = oxygen index.

occur probably as a result of the decomposition of organic carbon. Increases in ammonium (NH<sub>4</sub><sup>+</sup>) confirm this interpretation, but dissolved sulfate (SO<sub>4</sub><sup>2-</sup>) does not change noticeably. In the deeper sediments, alkalinities are well below the value of seawater, ammonium data are slightly elevated, but sulfate concentrations decrease to values well below that of seawater, mostly as a result of sulfate reduction. In Figure 14, the dilution-corrected concentrations of sulfate also are given. These estimates have been obtained through corrections based on observed decreases in dissolved chloride (see below, Fig. 14), assuming only dilutions of seawater concentrations (29 mM). The difference in the sulfate data indicates that the real sulfate concentrations are well below these estimates, again confirming that the sulfate reduction processes involve the decomposition of organic matter. Thus, at Site 914, the sulfate concentrations are reduced by about 7 mM, and at Site 915 by at least 4 to 5 mM. This amount of sulfate reduction is small and indicates that sulfate reduction was not yet complete in the sediment column when glacial action deposited the cap of glaciogenic sediments.

Data for alkaline earth elements are presented in Figure 14. In the upper glaciomarine sediments, rapid increases in calcium and equally rapid decreases in magnesium indicate respective release and uptake of these elements. This can be understood in terms of reactions involving the alteration of volcanic material in these sediments. The occurrence of intermixed tephra has been reported for the Site 914 sediments (see "Lithostratigraphy" section, "Site 914" chapter, this volume). Deeper in the sections at Sites 914 and 915, concentrations of both calcium and magnesium are approximately constant at about 30 mM. The concentrations of these elements are lower at Site 916, but a correction for potential dilution indicates that the concentrations of calcium might be roughly 33 mM, and similarly, concentrations of magnesium would be about 31 to 32 mM. Concentrations of dissolved strontium increase only slightly in the upper sediments; however, in the deeper sediment sections, distinct increases must have occurred. A study of the <sup>87</sup>Sr/<sup>86</sup>Sr composition of these deeper pore fluids will assist when determining the origin of this increase in dissolved strontium.

The alkali metals (sodium, potassium, and lithium) all show large changes with depth, as shown in Figure 14. In the upper glaciomarine sediments, concentrations of sodium (Na<sup>+</sup>) are somewhat higher than those in seawater (Na<sup>+</sup> ≈ 490 mM vs. Na<sup>+</sup> ≈ 480 mM in seawater), but at depth, a subtle decrease can be observed (e.g., at Site 914 at 218 mbsf, Na<sup>+</sup> ≈ 465 mM; and at Site 915, at about 178 mbsf, Na<sup>+</sup> ≈ 421 mM). The slight increases can be understood in terms of a small sodium release during alteration of volcanic glass in the upper sediments (similar to the increases observed in the upper sediments at Site 808; Gieskes et al., 1993). However, the decreases with depth must be the result of a minor uptake of sodium into authigenic minerals during alteration reactions. The major part of the sodium decrease

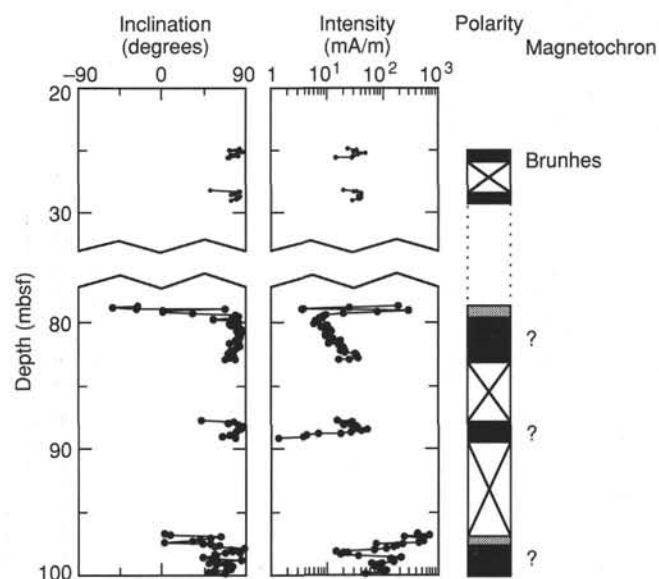


Figure 11. Summary of magnetostratigraphy of Hole 916A. In the polarity column, black = normal, shaded = indeterminate.

may be associated with the freshening of the interstitial waters with depth. This will be discussed further. Concentrations of potassium (K<sup>+</sup>) are depleted (compared with the seawater values) in the deeper sediment sections. Only a small part of this decrease can be explained by the observed freshening of the pore fluids, and most of the decreases result from an uptake into secondary minerals during alteration reactions involving the volcanogenic sediments (most likely into clay minerals). Concentrations of lithium decrease below seawater values in the upper glaciogenic sediments. This phenomenon also was observed in the upper sediment layers of Site 808 in the Nankai Trough (Gieskes et al., 1993). The most likely sink for this lithium is in alteration products of volcanic glass. In the deeper Paleogene sediments, subtle increases in lithium were observed that cannot be readily explained. However, in many sedimentary sections, initial decreases in lithium were followed by a release of lithium by the solid phases at somewhat elevated temperatures (>50°C).

Data for boron (B) and dissolved silica (H<sub>4</sub>SiO<sub>4</sub>) are presented in Figure 14. No spectacular changes in boron were observed, although in the deeper sections, values were seen to decrease below those of seawater. Dissolved silica values usually are representative of sediment types, confirming the different nature of the upper sediments from those of the deeper sediments.

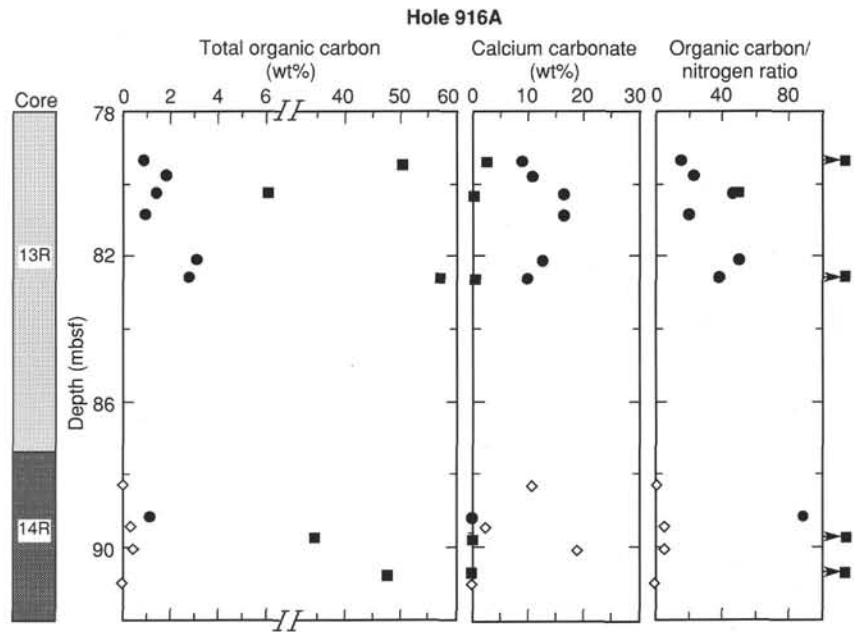


Figure 12. Plot of results of TOC, calcium carbonate (CaCO<sub>3</sub>), and TOC-TN ratio vs. depth in Cores 916A-13R and -14R. Note the change in the scale of the TOC diagram. The data are shown according to a preliminary lithologic distinction into sandy siltstones (solid circles), brown coal and peat (solid squares), and volcanic debris sediment (open symbols).

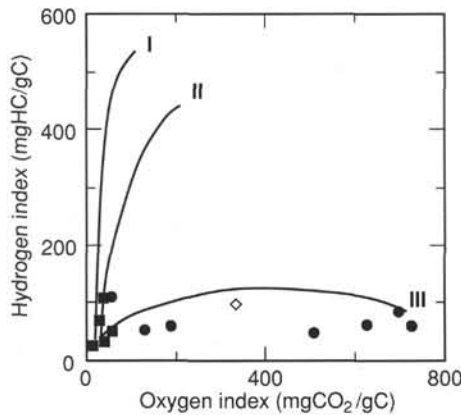


Figure 13. Results of the Rock-Eval pyrolysis of Hole 916A plotted in a "van Krevelen"-type diagram. Data point symbols as indicated in Figure 12. Kerogen types I and II are derived from aquatic algal material; type III indicates terrigenous organic matter.

The most interesting observations were the distinct decreases in dissolved chloride (Cl<sup>-</sup>) and salinity with depth (Fig. 14). Though only a subtle decrease was observed in the deeper sediments of Site 914, the decrease in chloride is essentially linear toward the basement (confirmed by the decreases in salinity). The decrease near the basalts is about 10% at Site 915, but at Site 916, chloride concentrations of as low as 405 mM were observed, signaling a change of 34% in the expected chloride concentration. Correlation plots between salinity and chloride and between sodium and chloride are presented in Figure 15A. In addition, Figure 15B presents a composite of the chloride data for all three sites. This composite suggests that the chloride anomaly becomes larger with the shallowing of basement. In turn, this may signify that low-salinity fluids trapped in the underlying basalts have accumulated mainly in the shallowest part of the basement complex.

**Summary and Conclusions**

The observations presented here are somewhat tentative, especially because of the relatively poor sediment recovery and the consequent inability to establish well-defined concentration-depth gra-

**Table 4. Chemical composition of interstitial waters at Site 916.**

Core, section, interval (cm)	Depth (mbsf)	Alkalinity (mM) pH	Salinity (g/kg)	Cl <sup>-</sup> (mM)	Ca <sup>2+</sup> (mM)	Mg <sup>2+</sup> (mM)	
152-916A-13R-3, 140-150	81.5	7.75	1.503	25	406	24.9	24.2

dients. Nonetheless, the data do allow us to make several observations and conclusions:

1. Effects of reactions involving the diagenesis of organic matter have left only minor signals in the interstitial waters of Sites 914, 915, and 916. This is evident from small increases in dissolved ammonium and a relatively small decrease in dissolved sulfate in the deeper sediment sections.
2. Alteration of volcanic material has caused small decreases in the concentration of magnesium in the upper 10 to 20 m of the sediment column. These decreases also are mirrored in small, but distinct, increases in calcium and, perhaps, strontium. The alteration of this material leads to a minor uptake of dissolved lithium, which shows a distinct depletion in concentration in the upper sediments.
3. The deeper, older sediment section is characterized by increases in dissolved calcium, strontium, and lithium (with a decrease in lithium toward the basement at Site 915). These increases are associated with decreases in magnesium and potassium. The concentration changes indicate that, prior to burial by rapidly deposited glaciogenic sediments, the sediment pore waters already were characterized by these signals, presumably as a result of the alteration of volcanic material. This interpretation needs to be confirmed by measuring the isotopic character of the dissolved strontium. Burial of these older sediments beneath the rapidly deposited glacial section may have slowed down diffusive communication with the overlying ocean. No distinct gradient of these components toward the basement is evident, except, perhaps, for strontium and lithium. This suggests that the signals have been created in the past by reaction of volcanic material in the sediments.
4. The steady linear decreases in dissolved chloride and salinity toward the basement, which are particularly well-documented in Site 915, indicate the possible presence of a fresher water reservoir in the originally subaerially exposed basalts. Diffusive influx of chloride (and associated ions) into this lower salinity reservoir then might

cause a decrease in dissolved chloride. A signal is particularly noticeable in chloride as a result of its high concentration, and because concentration of chloride can be estimated to an accuracy of better than 1%. If the flux actually occurred into a reservoir in the basement, this flux must have existed for a long time period (at least 30 m.y.), suggesting a substantial sink. Of course, the gradient in dissolved chloride may have steepened since the burial of the deeper sediments by the overlying glaciogenic sediment section. Studies of the oxygen and hydrogen isotopic compositions of the fluids will assist in the further evaluation of the origin of the fresh waters.

## PHYSICAL PROPERTIES

### Introduction

Following the drilling difficulties encountered with dropstones and diamicton at Sites 914 and 915, only coring with the RCB was attempted at Site 916. RCB-coring reduced the quality of the MST data and prevented continuous measurement of P-wave velocity. Recovery at Site 916 was not sufficient to form the basis of any detailed conclusion regarding the net downhole change in physical properties. However, the sample quality of some recovered sediments was good, and for these, a full suite of physical properties data was collected. Taken with the data from Sites 914 and 915, the physical properties data obtained from Site 916 are particularly useful for investigating the Quaternary glaciation along the East Greenland Shelf and the post-depositional compaction of both Quaternary and pre-Quaternary sediments.

### Multisensor Track (MST)

Only the more continuous sections were processed through the MST. Sections where stratigraphic continuity was lacking, such as where recovery consisted only of cobbles or isolated cored intervals through glacial boulders, were not processed. No continuous MST P-wave velocity measurements were performed at Site 916. GRAPE wet bulk density, magnetic susceptibility, and natural gamma data were collected for all MST runs. GRAPE wet bulk density data were corrected for drilling disturbance (reduced diameter), as detailed in the "Physical Properties" section of the "Explanatory Notes" chapter (this volume). A comparison between discrete and GRAPE bulk density demonstrates a correlatable difference of

$$y = 1.15x - 0.008, r^2 = 0.728, \quad (1)$$

where  $y$  = discrete wet bulk density, and  $x$  = GRAPE wet bulk density. This empirical correction factor of 1.15 is slightly less than the predicted factor of 1.18 (Boyce, 1976). All GRAPE bulk density measurements for Site 916 were corrected as per Equation 1. Composite MST plots are presented in Figure 16.

As outlined in the "Physical Properties" section of the "Site 914" chapter (this volume), the MST data set provides an excellent reference for evaluating the changes in bulk sediment composition and depositional environments. Cores from Site 916 have been interpreted in terms of mechanical units, as defined in the "Physical Properties" section, "Site 914" chapter (this volume).

The uppermost sediments (15.14–16.34 mbsf), recovered in Core 152-916A-3R, consist of a compact glacial diamicton that has been sandwiched between sets of cored clasts. These clasts (including dolerite, granitic gneiss, altered basalt, and diorite) probably were derived from surrounding diamicton. The highly variable magnetic susceptibility and natural gamma signatures for these clasts are important to note, as these features should be easily recognized from downhole logs and can be used to demonstrate stratigraphic continuity for the diamicton.

Diamicton, or its remnant clasts, also was recovered in Cores 152-916A-4R (24.3–25.6 mbsf) and -5R (28.0–29.5 mbsf). Section 152-916A-4R-1 contained only fragments of gabbro and amphibolite, giving high bulk densities (to  $>2.5 \text{ g/cm}^3$ ) and magnetic suscep-

tibility values (up to 2000 cgs units). Note that values for discrete clasts and boulder cores have not been plotted in Figure 16. Section 152-916-4R-2 consists largely of gravel at the top that grades into an indurated diamicton (24.9 mbsf) that is characterized by a bulk density of  $\approx 2.10 \text{ g/cm}^3$ , a magnetic susceptibility of  $\approx 500$  cgs, and by natural gamma in excess of 1100 TC. The decrease in magnetic susceptibility and bulk density from Sections 152-916-4R-1 to -4R-2 is accompanied by an increase in values of natural gamma (from about 500 to 1000 TC), presumably as a result of an increased number of granitic fragments in the gravel and diamicton. The MST data from Core 152-916A-5R show strong similarity with data from Sections 152-916A-4R-2 (24.9–25.6 mbsf) and -3R-1 (15.3–16.3 mbsf), and one may infer that the diamicton recovered represents one homogeneous stratigraphic unit (between 15 and 30 mbsf) that forms lithologic Subunit IB. The sediments in lithological Subunits IB and IC (see "Lithostratigraphy" section, this chapter) and their MST signatures indicate that they can be correlated with mechanical Unit M4, as defined for Site 914 (see "Physical Properties" section, "Site 914" chapter, this volume).

Sediments between 78 and 100 mbsf are primarily volcanogenic and correlate broadly with mechanical Unit M5, as defined for Site 914 (see "Physical Properties" section, "Site 914" chapter, this volume). Section 152-916A-13R-1 contains a calcite-cemented, silt sandstone between drilled fragments of basalt and sandstone clasts. The bulk density for the calcite-cemented sandstone is high ( $>2.50 \text{ g/cm}^3$ ). The underlying sections (152-916A-13R-2 and -3; 79.0–83.0 mbsf) consist of volcanogenic siltstones and sandstones having average bulk densities of  $1.80 \text{ g/cm}^3$  and natural gamma of  $\approx 800$  TC. The magnetic susceptibility for the intercalated siltstones and sandstones gradually increases with depth from  $<200$  cgs (at 79.5 mbsf) to 400 cgs (at 82.0 mbsf). An increase in grain density parallels this trend (see "Index Properties" section, below). This interval defines a coarsening-upward sequence, most likely with heavy, high magnetic susceptibility minerals that have been concentrated near the base. The base of Section 152-916A-13R-3 forms the top of a second coarsening-upward sequence that is consistent with a sharp increase in susceptibility values from 400 to  $>1500$  cgs units, and a much less significant increase in bulk density and natural gamma. This change is not mirrored in the visual appearance of the core, although we find that levels of opaque minerals are very high at this point (5%–10%). From the sedimentological and MST data, it seems likely that the lower part of this section represents a channel lag or a coarse-grained prograding unit.

The MST record for the interval from 87.7 to 91.0 mbsf (Core 152-916A-14R) shows significant variations in bulk density ( $1.40$ – $2.30 \text{ g/cm}^3$ ) and magnetic susceptibility (up to 2000 cgs units). The sediments consist of alternating silts and sands with polymict clasts. Downcore, the magnetic susceptibility decreases to a minimum value, which correlates with increasing organic content and culminates at a prominent woody layer at 89.0 mbsf (magnetic susceptibility minimum of  $<25$  cgs). Bulk density also reaches a local minimum value here, while the natural gamma signal displays a sharp break, indicating a marked change in sediment geochemistry (e.g., sediments above and below 89.0 mbsf are from different source regions). The natural gamma signal below this layer is consistently lower ( $<700$  TC) than that of the overlying sediments. Toward the base of Core 152-916A-14R, clasts become more abundant with numerous altered basaltic scoriaceous fragments and boulders that produce a spiked, magnetic susceptibility signal.

The MST data from the deepest core (152-916A-15R) recovered at Site 916 are similar in character to those recorded from Core 152-914A-14R (Fig. 15, "Physical Properties" section "Site 914" chapter, this volume) and show large swings in magnetic susceptibility ( $>3000$  cgs units). This variability reflects the diverse and poorly sorted sediment assemblage associated with a volcanic debris flow.

Taking the volcanogenic sequence as a whole (Cores 152-914A-13R to -15R), a marked and consistent increase in magnetic suscepti-

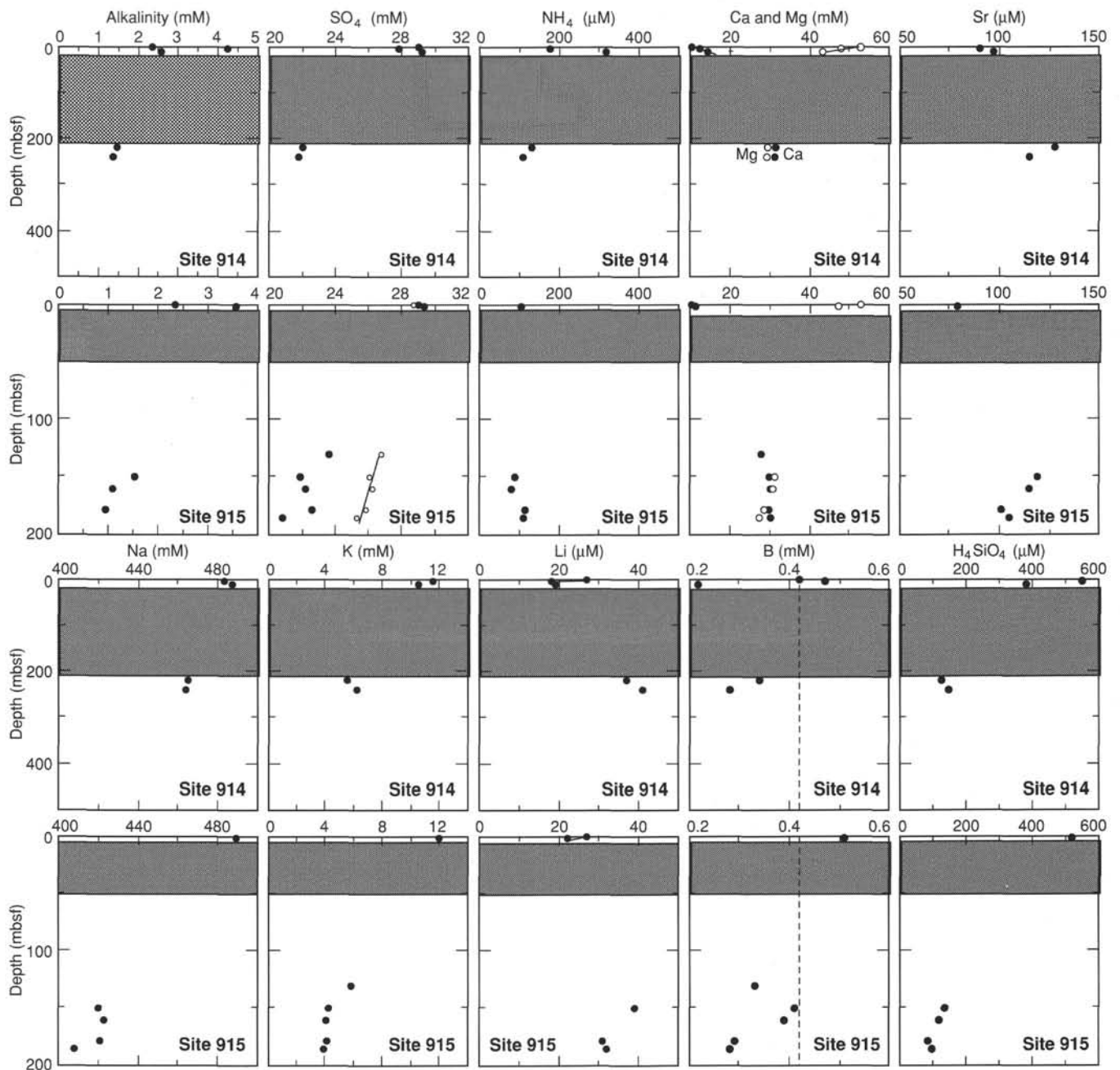


Figure 14. Distribution of alkalinity, sulfate, ammonium, alkaline earth elements (Ca, Mg, Sr), alkali metal ions (Na, K, Li), boron, silica, salinity, and chloride. Small open circles in the sulfate graph of Site 915 indicate concentrations based on calculations that resulted from the observed freshening of the pore fluids (see text). Shaded area indicates the glaciogenic section.

bility, from 200 cgs (at 79.5 mbsf) to 2100 cgs (at 99.0 mbsf), is seen. A parallel, gradual decrease in natural gamma also occurs over the whole of this interval, but is less pronounced. However, at a depth of 89 mbsf, the natural gamma signal decreases rapidly (from 800 to <700 TC) and is maintained at this lower value for the remaining sediments.

### Index Properties

Values of wet bulk density, grain density, dry density, water content, porosity, and void ratio (see "Physical Properties" section, "Explanatory Notes" chapter, this volume) have been determined for 17 discrete samples. These data are tabulated in Table 5 and illustrated in Figure 16.

The wet bulk density of the shallow diamicton (mechanical Unit M4) is in good agreement with the values obtained for Unit M4 at Hole 914A. The bulk density within Unit M4 at Site 916 decreases from 2.39 g/cm<sup>3</sup> (at 16.0 mbsf) to 2.21–2.23 g/cm<sup>3</sup> (25.5–29.0 mbsf). Grain density remains almost constant (2.80 g/cm<sup>3</sup>) throughout the diamicton, while the water content increases from 14% (at 16.0 mbsf) to 20% (at 26.0 mbsf). This is the reverse of the trend in water content found in Unit M4 at Site 914.

The decrease in bulk density continues downcore, with a mean value of 1.95 g/cm<sup>3</sup> in the volcanogenic sands and silts between 79.0 and 98.0 mbsf. For all the sediments at Site 916, grain density value remains almost constant at 2.80 g/cm<sup>3</sup>. A significant increase in grain density is apparent through 80.0 to 83.0 mbsf, in parallel with an in-

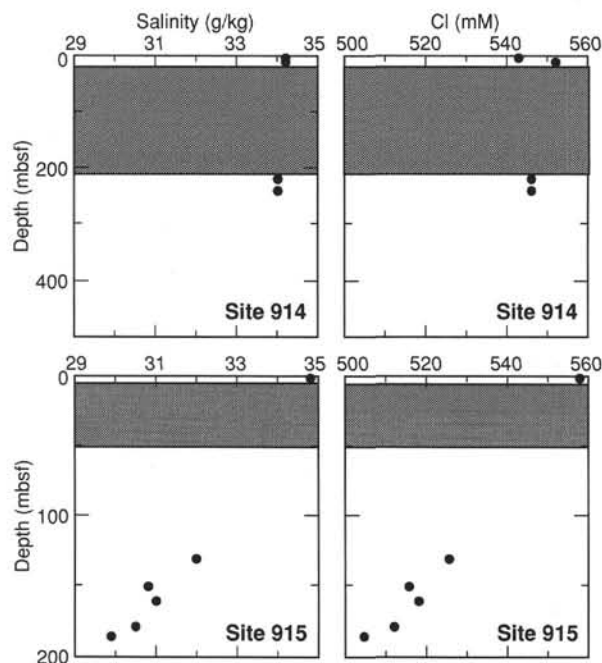


Figure 14 (continued).

crease in magnetic susceptibility. This is almost certainly the result of an increase in the abundance of fine-grained opaque minerals and oxides.

### Velocimetry

Hamilton Frame compressional ( $P$ -wave) velocity measurements were acquired for 22 discrete sediment cubes that were removed from Cores 152-916A-3R to -5R and -13R to -15R. Velocities were measured in three directions: longitudinal ( $V_z$ ), transverse ( $V_x$ ), and transverse ( $V_y$ ) (see "Physical Properties" section, "Explanatory Notes" chapter, this volume). Data are presented in Table 6 and illustrated in Figures 17A and 17B. No digital sonic velocimeter (DSV) data were collected at Site 916, as the sediments were too indurated for insertion of the transducers.

Acoustic velocity for the compact diamicton (lithologic Subunit IB, mechanical Unit M4, Cores 152-916-3R to -5R; 15.0–25.0 mbsf) decreases with depth from 2.25 to 1.85 km/s. This correlates with a reduction in discrete bulk density (from 2.39 to 2.21 g/cm<sup>3</sup>), and an increase in water content (from 14% up to 20%). The grain density remains constant at 2.83 g/cm<sup>3</sup>.

Sediments recovered from lithologic Unit II (Cores 152-916A-13R and -14R; 78–91 mbsf) consist of volcanogenic sands, silts, and conglomerates. On the basis of their acoustic nature, these sediments may be subdivided into four genera (Fig. 17B): (1) acoustically anisotropic, medium sonic velocity (1.90 km/s), volcanogenic sandy silts; (2) high to very high sonic velocity (up to 4.35 km/s), strongly anisotropic, carbonate-cemented volcanogenic silty sands; (3) high sonic velocity (2.00–2.20 km/s) laminated volcanogenic silts; and (4) medium sonic velocity (1.95 km/s), acoustically isotropic, highly attenuating conglomerates.

The sonic velocity for the lowermost (97.0–99.0 mbsf), poorly bedded, proximal volcanoclastic sediments and debris flows of lithologic Unit III is considerably slower (1.80 km/s) than that of the overlying sediments (1.95 km/s) of lithologic Unit II. Clearly, these sediments are isotropic (Fig. 17B) and severely attenuate the passing signal. The slower velocities reflect the poorly sorted and highly weathered nature of the sediments.

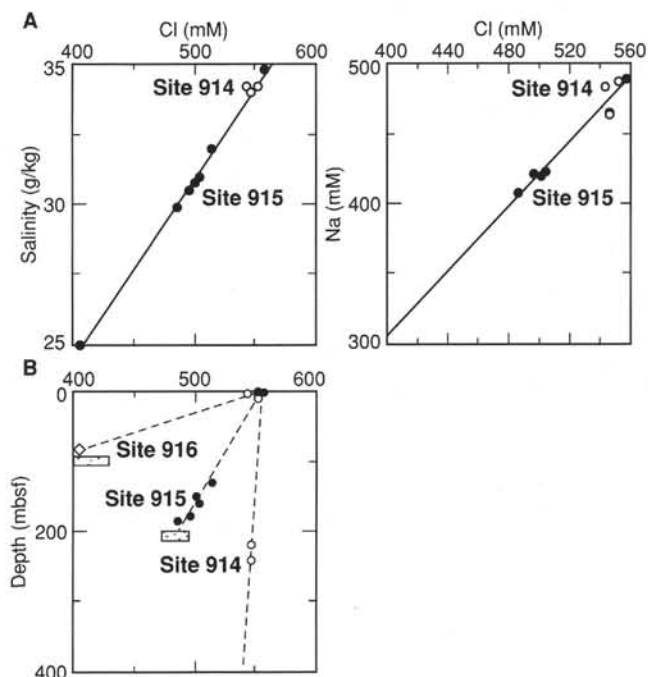


Figure 15. **A.** Correlations between chloride and salinity, and chloride and sodium at Site 914 (open circles), 915 (solid circles), and 916 (open diamonds). **B.** Composite plot of chloride concentration vs. depth for Sites 914–916. Stippled area indicates basement rock.

### Undrained Shear Strength

In Cores 152-916A-4R, -5R, and -6R, discontinuous diamicton was recovered from 10.0 to 30.0 mbsf at Site 916. The extremely indurated and compacted nature of these diamictons precluded insertion of the minivane. Using a handheld penetrometer, a number of attempts were made to determine the shear strength of the diamicton, but the strength lay beyond the range of the instrument (i.e., >4.5 kg/cm<sup>2</sup>). The degree of this compaction is supported by the high acoustic velocities (>1.9 km/s) and bulk densities (2.20–2.40 g/cm<sup>3</sup>) and by the very low water content (<15%) associated with the diamicton.

As experienced at Sites 914 and 915, indurated sediments recovered from the deeper, volcanoclastic sediments in Cores 152-916A-9R through -15R were prone to either brittle failure in the silty sediments or, in sandy sediments, had strengths beyond the range of the penetrometer.

### Thermal Conductivity and Electrical Resistivity

Thermal conductivity measurements are listed in Table 12, "Physical Properties" section, "Site 914" chapter (this volume) and illustrated in Figure 18, "Physical Properties" section, "Site 914" chapter (this volume). Thermal conductivities in the upper sediments (lithologic Units I and II) range from 0.82 to 1.59 W/(m-K), with an average value of 1.14 W/(m-K). The thermal conductivity profile shows two low zones of 1.11 W/(m-K) (79.0–81.0 mbsf) and 0.84 W/(m-K) (97.0–98.0 mbsf) in lithologic Unit II. This change correlates with CaCO<sub>3</sub> cementation.

No electrical resistivities were measured because the indurated nature of the sediments prevented insertion of the resistivity probes.

### Summary

On the basis of physical properties data, the sediments recovered at Site 916 may be correlated with the mechanical units scheme

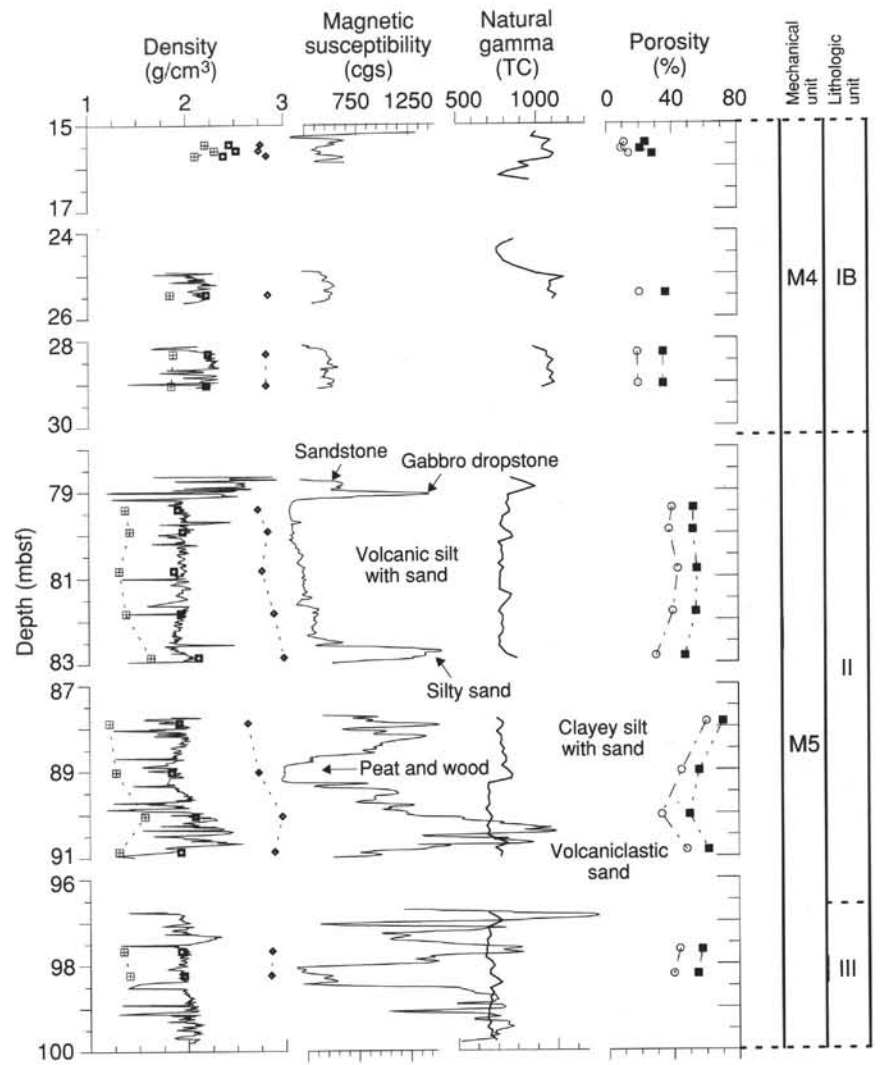


Figure 16. Composite plot of MST and discrete index-property data for sediments recovered at Site 916. MST data comprise GRAPE wet-bulk density (corrected for reduced diameter as a result of RCB-coring; see "Physical Properties" section, "Explanatory Notes" chapter, this volume), magnetic susceptibility, and natural gamma. Discrete measurements include wet bulk density (open squares), grain density (open diamonds), dry density (hachured squares), water content (open circles), and porosity (filled squares).

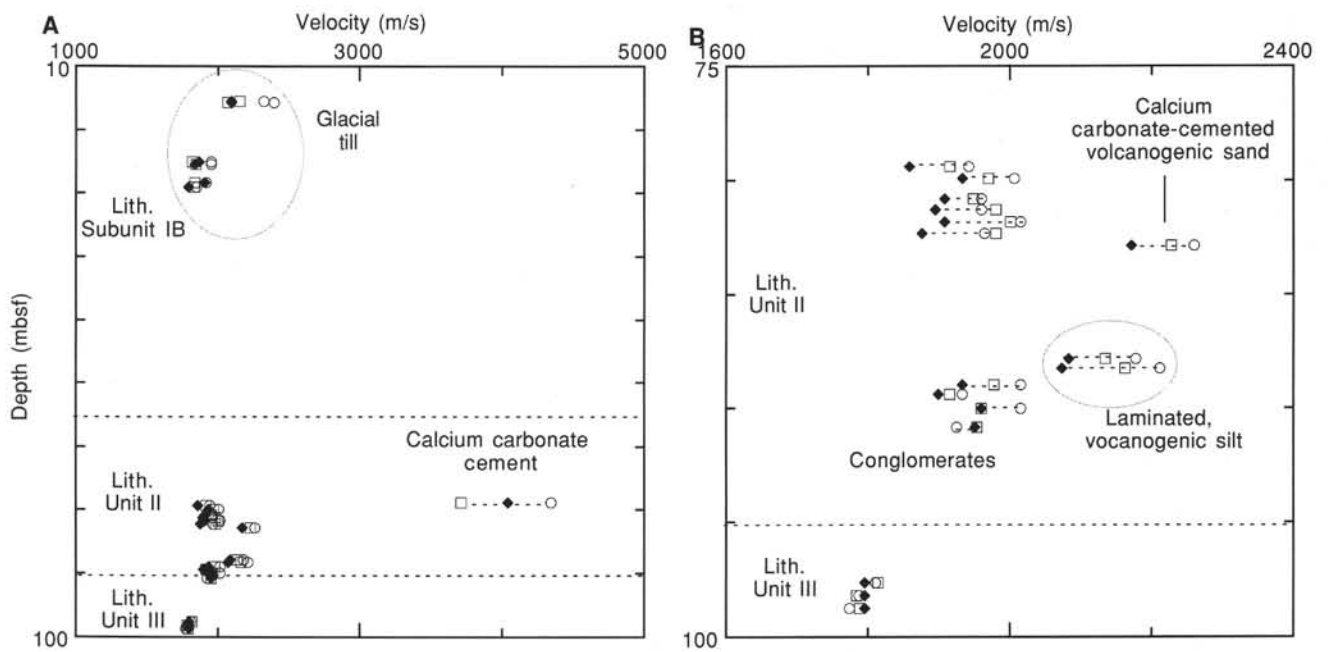


Figure 17. Discrete longitudinal ( $V_z$  = solid diamonds) and transverse sonic velocities ( $V_x$  = open squares and  $V_y$  = open circles) for sediments recovered in Hole 916A. A. All data. B. Selected data at a larger scale.

Table 5. Index property data for Site 916.

Core, section, interval (cm)	Depth (mbsf)	Water content $W_i$ (%)	Bulk density (g/cm <sup>3</sup> ) (MB)	Grain density (g/cm <sup>3</sup> ) (MC)	Dry density (g/cm <sup>3</sup> ) (MB)	Porosity (%) (MC)	Void ratio (MC)
152-916A-							
3R-1, 25-27	15.35	11.10	2.45	2.77	2.20	23.90	0.30
3R-1, 50-52	15.60	9.20	2.52	2.75	2.30	20.90	0.20
3R-1, 62-64	15.72	13.82	2.39	2.83	2.10	28.34	0.38
4R-2, 56-58	25.45	20.16	2.21	2.84	1.84	36.20	0.56
5R-1, 21-23	28.31	18.89	2.23	2.82	1.87	34.58	0.52
5R-1, 93-95	29.03	19.13	2.21	2.82	1.85	34.59	0.53
13R-1, 80-82	79.40	39.45	1.91	2.73	1.37	52.72	1.05
13R-1, 132-134	79.92	37.74	1.96	2.83	1.42	52.44	1.04
13R-2, 73-75	80.83	43.04	1.87	2.77	1.31	54.92	1.16
13R-3, 22-24	81.82	40.17	1.94	2.89	1.38	54.24	1.14
13R-3, 125-127	82.85	29.81	2.12	2.99	1.63	47.54	0.87
14R-1, 18-20	87.88	60.35	1.92	2.62	1.20	70.58	1.54
14R-1, 132-134	89.02	45.14	1.84	2.73	1.27	55.85	1.20
14R-2, 83-85	90.03	32.78	2.08	2.97	1.56	50.04	0.95
14R-3, 15-17	90.85	48.15	1.93	2.89	1.30	61.35	1.36
15R-2, 63-65	97.66	43.87	1.93	2.86	1.34	57.52	1.22
15R-2, 120-122	98.23	39.98	1.96	2.85	1.40	54.68	1.11

Note: Data were calculated according to Method B (MB) or Method C (MC) as defined in "Physical Properties" section, "Explanatory Notes" chapter (this volume).

established at Site 914 (see "Physical Properties" section, "Site 914" chapter, this volume). Mechanical Units M1, M2, and M3, which correspond to lithological Subunit IA (see "Lithostratigraphy" section, "Site 914" chapter, this volume) were not recovered at Site 916. As these units have been described in the upper 5 m of the sediment column at Site 914 and were only partially recovered at Site 915, their absence at Site 916 is not surprising, because coring with the RCB is not effective for recovering nonindurated sediments.

Mechanical Unit M4 is a highly compacted and indurated diamicton that correlates to lithological Subunit IB. Unit M4 is characterized by relatively high acoustic velocity ( $\approx 2.1$  km/s), high bulk density (2.20–2.40 g/cm<sup>3</sup>), low water content (<20%), and by the spiked nature of the GRAPE bulk density, magnetic susceptibility, and natural gamma data. These spikes result from the numerous, lithologically diverse assemblages of clasts. The inverted velocity, bulk density, and water content profiles for this unit are of particular interest. We suggest that such surficial compaction may have resulted from horizontal shear stresses that were imposed by the advance of glacial ice over a hydrostatically supported sediment column. Were this advance and retreat sufficiently rapid, the deeper sediment would not have had time to dewater and thus would have remained less consolidated than the overlying, horizontally stressed upper diamicton.

The deeper sediments (46.0–100.0 mbsf), interbedded, indurated volcanogenic silts and sands, are grouped into mechanical Unit M5 and correlate with lithologic Units II and III (see "Lithostratigraphy" section, this chapter). The interbedded sands and silts show considerable variations in MST data over short depth intervals. These variations relate to factors such as cementation, grain size, sorting, and provenance. At Site 916, the MST data from mechanical Unit M5 record a continuous downcore increase in magnetic susceptibility. In conjunction with the sedimentological data, it appears that this trend is the result of an increase in the weathering of basaltic material toward the basement (i.e., the sediment source area gradually became dominated by more basaltic rocks). A slow, but steady, decrease in natural gamma toward the basement may reflect the coarser nature of the basal sediments and/or whether a depositional regime less rich in potassium (continental?) detritus were available. Natural gamma spikes, superimposed on this general trend (e.g., 89.0 mbsf), most probably represent

Table 6. P-wave velocity measurements for Site 916.

Core, section, interval (cm)	Depth (mbsf)	Calculated velocity			Comments
		$V_z$ (m/s)	$V_x$ (m/s)	$V_y$ (m/s)	
152-916A-					
3R-1, 25-27	15.45	2094	2151	2321	Diamicton
3R-1, 62-64	15.72	2093	2068	2392	Diamicton
4R-2, 13-15	25.02	1866	1816	1952	Diamicton
4R-2, 56-58	25.45	1834	1843	1952	Diamicton
5R-1, 21-23	28.31	1908	1834	1916	
5R-1, 93-95	29.03	1790	1830	1850	Small clast at top
13R-1, 30-32	78.90	4041	3714	4346	Calcite cemented sst
13R-1, 80-82	79.40	1858	1915	1942	Ash origin
13R-1, 132-134	79.92	1933	1970	2006	Ash origin
13R-2, 73-75	80.83	1908	1949	1960	Volcaniclastic sandy silt
13R-2, 118-120	81.28	1895	1981	1960	Volcaniclastic sandy silt
13R-3, 22-24	81.82	1908	2001	2015	Volcaniclastic sandy silt
13R-3, 72-74	82.32	1876	1981	1965	Volcaniclastic silt
13R-3, 125-127	82.85	2172	2228	2260	Volcaniclastic sst
14R-1, 17-19	87.87	2083	2135	2178	Laminated silt
14R-1, 156-158	88.26	2073	2163	2212	
14R-1, 131-135	89.01	1933	1978	2015	
14R-2, 21-23	89.41	1899	1915	1933	Silts with clasts
14R-2, 82-84	90.02	1960	1960	2015	Homogeneous silts
14R-3, 14-16	90.84	1951	1954	1925	Volcaniclastic ash breccia
15R-2, 63-65	97.66	1796	1815	1811	No bedding
15R-2, 119-121	98.22	1796	1784	1788	Silts with clasts
15R-3, 31-33	98.77	1796	1789	1774	Silts with clasts

Note: Longitudinal velocity  $V_z$  is perpendicular to core axis, transverse velocity  $V_x$  is parallel to bedding strike, transverse velocity  $V_y$  is perpendicular to bedding strike (see "Physical Properties" section, "Explanatory Notes" chapter, this volume). sst = silty sandstone.

the sudden influx of cratonic detritus as a result of an enlarged basin/catchment area.

Discrete variations in compressional ( $P$ -wave) velocities result from increased cementation. A velocity inversion is present at the division between lithologic Units II and III, which reflects the weathered and poorly sorted nature of the basal sediments.

#### Ms 152IR-108

**NOTE:** For all sites drilled, core-description forms ("barrel sheets") can be found in Section 4, beginning on page 303. Forms containing smear-slide data can be found in Section 5, beginning on page 925. GRAPE, Index property, MAGSUS and Natural gamma-ray data are presented on CD-ROM (back pocket).